J. Fluid Mech. (2003), *vol.* 482, *pp.* 207–233.
DOI: 10.1017/S002211200300404X Printed in the United Kingdom

Equilibrium states of turbulent homogeneous buoyant flows

By L. H. JIN[1], R. M. C. SO[2] AND T. B. GATSKI[3]

[1]Department of Engineering Mechanics, Tsinghua University, Beijing 100084, PR China

[2]Department of Mechanical Engineering, The Hong Kong Polytechnic University, Hung Hom, Kowloon, Hong Kong

[3]Computational Modeling and Simulation Branch, NASA Langley Research Center, Hampton, VA 23681-2199, USA

(Received 15 April 2002 and in revised form 6 January 2003)

The equilibrium states of homogeneous turbulent buoyant flows are investigated through a fixed-point analysis of the evolution equations for the Reynolds stress anisotropy tensor and the scaled heat flux vector. The mean velocity and thermal fields are assumed to be two-dimensional. Scalar invariants formed from the Reynolds stress anisotropy tensor, the scaled heat flux vector, and the strain rate and rotation rate tensors are governed by a closed set of algebraic equations derived for the stress anisotropy and scaled heat flux under a (weak) equilibrium assumption. Six equilibrium state variables are identified for the buoyant case and contrasted with the corresponding two state variables obtained for the non-buoyant homogeneous turbulence case. These results, while dependent on the functional forms of the models for the pressure–strain rate correlation tensor and the pressure–scalar-gradient correlation and viscous dissipation vector, can be used as in the non-buoyant case to either calibrate new closure models or validate the performance of existing models. In addition, since the analysis only involves the turbulent time scales (both velocity and thermal) and their ratio, the results of the analysis are independent of the specific models for the dissipation rates of the turbulent kinetic energy and the temperature variance. The analytical results are compared with model predictions as well as recent direct numerical simulation (DNS) data for buoyant shear flows. Good agreement with DNS data is obtained.

1. Introduction

Homogeneous turbulent flows play a central role in the modelling and analysis of complex inhomogeneous flows because they can provide a great deal of insight into the key parameters characterizing turbulence in a simplified setting. With suitable assumptions, these simplified cases quite often give rise to closed-form solutions to the governing equations when commonly used turbulence models are invoked. As a result, homogeneous turbulent flows have been investigated extensively (see e.g. Rogallo & Moin 1984; Reynolds 1990; Speziale 1991). These investigations provided much-needed insight into the understanding of the evolution of homogeneous turbulence and its approach to equilibrium. In the area of turbulent buoyant shear flows, direct numerical simulations (DNS) have been performed by Gerz, Schumann & Elghobashi (1989), Gerz & Schumann (1991), Kaltenbach, Gerz & Schumann (1994), Jacobitz, Sarkar & Van Atta (1997), Jacobitz & Sarkar (1998) and Shih *et al.* (2000), whereas

Sirivat & Warhaft (1983), Stillinger, Helland & Van Atta (1983), Itsweire, Helland & Van Atta (1986), Rohr *et al.* (1988) and Piccirillo & Van Atta (1997) carried out experimental investigations to examine the effect of buoyancy on homogeneous stratified turbulence. Sommer & So (1995) and Sommer, So & Zhang (1997) have examined turbulence modelling effects on the prediction of internal gravity waves and counter-gradient heat flux. According to these investigations, stable stratification weakens isotropization, implying that an isotropic dissipation rate model (Kolmogorov 1941) is not adequate to describe the evolution of buoyant homogeneous turbulence. Recently, So, Zhao & Gatski (1999) conducted a numerical study using different turbulence models and assessed the performance of certain anisotropic dissipation rate models. This study revealed that difficulties still persisted in the prediction of counter-gradient heat flux and the onset of internal gravity waves in buoyant shear flows. While such studies have been useful in identifying inherent weaknesses in existing buoyancy models, it has not been possible to develop improved alternatives, partly because these studies were confined to a short time period (or near-field region for experiments) and were dependent on the initial state.

An important property of homogeneous turbulent flows is the appearance of dynamic state variables that tend to approach equilibrium values in the long time limit. The equilibrium states provide an important benchmark in the calibration of closure models. For homogeneous turbulent flows without buoyancy effects, the fixed points associated with the equilibrium can be determined (Speziale & Mac Giolla Mhuiris 1989; Speziale, Sarkar & Gatski 1991). These fixed points can then be used to assess the suitability of higher-order models and their ability to predict the correct equilibrium values. For example, Abid & Speziale (1993) calculated the equilibrium states for homogeneous turbulent shear flow and channel flow using Reynolds stress closures in order to assess their predictive performance.

Recently, Jongen & Gatski (1998), using projection methodology, derived a general algebraic relation between the production-to-dissipation rate ratio, $\tilde{P}/\varepsilon$, and the mean-to-turbulent time-scale ratio, Sk/ε, based solely on the form of the pressure–strain rate model, and without recourse to a modelled ε-equation. Here, $\tilde{P}$ is the mean shear production of the turbulent kinetic energy, k, ε its dissipation rate, and S the mean shear rate. The analysis gave the same equilibrium values as those predicted by an appropriate Reynolds stress turbulence closure. Furthermore, the authors concluded that the exact form of the ε-equation was not important for predicting the equilibrium states of turbulent shear flows since it only entered indirectly through the ratio Sk/ε.

Tavoularis & Corrsin (1981) conjectured that equilibrium states also exist for buoyant shear flows; however they take a longer time (or distance) to achieve due to the interaction between shear and buoyancy. The approach to equilibrium turbulence for buoyant shear flow is much more complicated. Even the parameters that characterize the equilibrium states are to date not known precisely. Recently, Zhao, So & Gatski (2001) investigated the effects of turbulence modelling on the prediction of equilibrium states of buoyant shear flows. They concluded that the choice of models for ε and the temperature variance dissipation rate ε_θ was very important for the prediction of equilibrium states, and not all models could predict an approach to equilibrium. Unfortunately, it was not possible from the available data to determine why some of the models tested performed poorly, although, some inconsistencies may exist between the formulation for the temperature variance $\overline{\theta^2}$ and its dissipation rate equation.

Numerical modelling of buoyant flows, even under the assumption of incompressibility, is much more complicated than the non-buoyant case due to the coupling

between the velocity and the temperature field. In addition to closure models for the Reynolds stress equation, models for the Reynolds heat flux, the k and k_θ and their associated ε and ε_θ equations need to be invoked (Launder 1978, 1989). Furthermore, buoyancy effects should also be modelled in the pressure–strain rate term based on the argument that buoyancy forces are present in the Poisson equation for the fluctuating pressure and hence contribute to the redistribution process governed by the pressure–strain rate correlation. A modelled buoyancy term is also added to the ε-equation to account for buoyancy effects in the calculation of ε. It should be noted that this treatment of buoyancy effects on the turbulence field is rather incomplete, because the interaction between shear and buoyancy is highly nonlinear. Also the modelling of ε_θ may not correctly reflect the modelling of the pressure–scalar-gradient correlation or pressure–scrambling term, and thus an inconsistency between them may exist as well. Unfortunately, within the current framework it is only possible to quantify such inconsistencies when some independent measure of the equilibrium states of these buoyant homogeneous flows is obtained. If such results could be obtained from physical and/or numerical experiments, then the analysis outlined here could be used to optimize the choice of closure coefficients such as those in the modelled ε_θ-equation.

Indeed, the modelled evolution equations for the Reynolds stress anisotropy and the scaled heat flux vector can be solved numerically to equilibrium, thus allowing the equilibrium states of homogeneous buoyant turbulence to be determined (Zhao *et al.* 2001). This process does not yield the required relationships between the equilibrium state variables that are necessary for an optimization of the choice of closure coefficients of buoyant turbulence. With so many equilibrium state variables involved, it would be difficult, if not impossible, to determine the relationships among them. In principle, these relationships could be deduced from an extensive collection of results from the numerical solution of the relevant modelled equations, but it would be a tedious process to map out the whole parameter space that involved so many state variables. The projection methodology employed to analyse the relevant equations rigorously identifies the state variables that are fixed points of the system and shows their relationship to one another. This idea of projection was first proposed in continuum mechanics (Rivlin & Ericksen 1955) and it has been successfully applied to analyse equilibrium states of incompressible homogeneous turbulence (Jongen & Gatski 1998).

Therefore, in the current study, the modelled transport equations for buoyant turbulence, i.e. the Reynolds stress anisotropy and the scaled heat flux vector equations, are analysed through the projection methodology used previously in Jongen & Gatski (1998). Once again, corresponding algebraic models are not needed and are not developed. Instead, the equilibrium state of homogeneous buoyant flows, as determined from a rather general form of the modelled evolution equations, is analysed. As is now well-accepted in the turbulence modelling community, calibration based on equilibrium-state behaviour is an acceptable and desirable means of model calibration. This too is demonstrated in the current study where some obvious requirements imposed on the modelling coefficient are identified. The only 'models' being validated are the commonly accepted rather general forms of modelled terms such as the pressure–scrambling vector.

2. Evolution of the Reynolds stress anisotropy

The flow to be considered is a homogeneous, buoyant turbulent flow where the Boussinesq approximation is assumed to be valid. Invoking this assumption, the

modelled incompressible Reynolds-stress equation can be written as (So *et al.* 2002)

$$\frac{\mathrm{d}\overline{u_i u_j}}{\mathrm{d}t} = P_{ij} + \Pi_{ij} - \varepsilon_{ij} + G_{ij}, \tag{1}$$

where u_i is the ith component of the fluctuating velocity, $\overline{u_i u_j}$ is the kinematic Reynolds stress tensor, $P_{ij} = -\overline{u_i u_k}(\partial U_j/\partial x_k) - \overline{u_j u_k}(\partial U_i/\partial x_k)$ is the shear stress production tensor, $\varepsilon_{ij} = 2\nu\overline{(\partial u_i/\partial x_k)(\partial u_j/\partial x_k)}$ is the dissipation rate tensor, $G_{ij} = -\beta g_i \overline{u_j\theta} - \beta g_j \overline{u_i\theta}$ is the buoyant production tensor of the Reynolds stresses, $\overline{u_i\theta}$ is the turbulent heat flux vector, β is the coefficient of thermal expansion of the fluid, $g_i = (0, 0, g_3) = (0, 0, -g_c)$ is the gravitational vector and $\mathrm{d}/\mathrm{d}t$ is the time derivative. Only the pressure-strain rate tensor Π_{ij} and ε_{ij} in (1) require modelling.

In order to close (1), a rather general form for the pressure–strain rate correlation tensor can be assumed and is written for buoyant flows as

$$\begin{aligned}\Pi_{ij} = &-\left(C_1^0 + C_1^1\frac{\tilde{P}}{\varepsilon}\right)\varepsilon\, b_{ij} + C_2 k S_{ij} + C_3 k\left(b_{ik}S_{kj} + S_{ik}b_{kj} - \tfrac{2}{3}b_{mn}S_{mn}\delta_{ij}\right)\\ &- C_4 k(b_{ik}W_{kj} - W_{ik}b_{kj}) + C_5\varepsilon\left(b_{ik}b_{kj} - \tfrac{1}{3}b_{mn}b_{nm}\delta_{ij}\right) - C_6\left(G_{ij} - \tfrac{2}{3}G\delta_{ij}\right),\end{aligned} \tag{2}$$

where $b_{ij} = (\overline{u_i u_j}/2k - \delta_{ij}/3)$ is the Reynolds stress anisotropy tensor, $\tilde{P} = P_{ii}/2$ is the shear stress production of k, and $G = G_{ii}/2$ is the buoyant production of k. The closure constants C_i will be assigned later when the different homogeneous flows are discussed. Note that the effect of buoyancy on Π_{ij} is accounted for by the last term in (2). The kinematic strain rate tensor S_{ij} and the rotation rate tensor W_{ij} are defined as $S_{ij} = (\partial U_i/\partial x_j + \partial U_j/\partial x_i)/2$ and $W_{ij} = (\partial U_i/\partial x_j - \partial U_j/\partial x_i)/2$, respectively.

For buoyant shear flows, an equation for b_{ij} can be derived using the following identity:

$$\frac{\mathrm{d}b_{ij}}{\mathrm{d}t} = \frac{1}{2k}\left(\frac{\mathrm{d}\overline{u_i u_j}}{\mathrm{d}t} - \frac{\overline{u_i u_j}}{k}\frac{\mathrm{d}k}{\mathrm{d}t}\right). \tag{3}$$

Substituting (1) and its trace equation into (3) gives

$$\begin{aligned}\dot{b}_{ij} = \frac{\mathrm{d}b_{ij}}{\mathrm{d}t} = &\frac{\varepsilon}{k}\left(1 - \frac{\tilde{P}}{\varepsilon} - \frac{G}{\varepsilon}\right)b_{ij} - \tfrac{2}{3}S_{ij} - \left(b_{ik}S_{kj} + S_{ik}b_{kj} - \tfrac{2}{3}b_{mn}S_{mn}\delta_{ij}\right)\\ &+ (b_{ik}W_{kj} - W_{ik}b_{kj}) + \frac{1}{2k}\Pi_{ij} - \frac{\varepsilon}{k}d_{ij} + \frac{1}{2k}\left(G_{ij} - \tfrac{2}{3}G\delta_{ij}\right),\end{aligned} \tag{4}$$

where d_{ij} is the dissipation rate anisotropy defined as $d_{ij} = (\varepsilon_{ij}/2\varepsilon - \delta_{ij}/3)$. Thus, $d_{ij} = 0$ corresponds to the Kolmogorov (1941) isotropic model for ε_{ij}. Using the SSG pressure–strain model given in (2), the general form of the differential equation for b_{ij} becomes

$$\begin{aligned}\dot{b}_{ij} = &-\frac{1}{g\lambda}b_{ij} - a_1 S_{ij} - a_3\left(b_{ik}S_{kj} + S_{ik}b_{kj} - \tfrac{2}{3}b_{mn}b_{mn}\delta_{ij}\right) + a_2(b_{ik}W_{kj} - W_{ik}b_{kj})\\ &+ \frac{1}{\lambda}a_4\left(b_{ik}b_{kj} - \tfrac{1}{3}b_{mn}b_{mn}\delta_{ij}\right) - \frac{1}{\lambda}d_{ij} - \frac{a_6}{2k}\left(G_{ij} - \tfrac{2}{3}G\delta_{ij}\right),\end{aligned} \tag{5}$$

where $\lambda = k/\varepsilon$ and

$$\frac{1}{g} = \left(\frac{C_1^1}{2} + 1\right)\left(\frac{\tilde{P}}{\varepsilon}\right) + \frac{G}{\varepsilon} + \left(\frac{C_1^0}{2} - 1\right) = a_0^0\left(\frac{\tilde{P}}{\varepsilon}\right) + \frac{G}{\varepsilon} + a_0^1, \tag{6}$$

with $a_1 = (4/3 - C_2)/2$, $a_2 = (2 - C_4)/2$, $a_3 = (2 - C_3)/2$, $a_4 = C_5/2$, $a_6 = C_6 - 1$. Under the condition of $\dot{b}_{ij} = 0$ at equilibrium, (5) can be written in matrix notation as

$$-\frac{1}{g\lambda}\boldsymbol{b} - a_3\left(\boldsymbol{bS} + \boldsymbol{Sb} - \tfrac{2}{3}\{\boldsymbol{bS}\}\boldsymbol{I}\right) + a_2(\boldsymbol{bW} - \boldsymbol{Wb}) + \frac{a_4}{\lambda}\left(\boldsymbol{b^2} - \tfrac{1}{3}\{\boldsymbol{b^2}\}\boldsymbol{I}\right) = a_1\boldsymbol{S} + \boldsymbol{L}, \tag{7}$$

where $\boldsymbol{I}$ is the identity tensor and

$$\boldsymbol{L} = \frac{1}{\lambda}\left[\boldsymbol{d} + a_6\left(\frac{G}{\varepsilon}\right)\boldsymbol{F}\right], \tag{8a}$$

$$\boldsymbol{F} = \frac{\boldsymbol{G}}{2G} - \frac{\boldsymbol{I}}{3}. \tag{8b}$$

Equation (7) can be written in a dimensionless form as

$$-\frac{1}{g}\boldsymbol{b} - a_3\left(\boldsymbol{bS}^* + \boldsymbol{S}^*\boldsymbol{b} - \tfrac{2}{3}\{\boldsymbol{bS}^*\}\boldsymbol{I}\right) + a_2(\boldsymbol{bW}^* - \boldsymbol{W}^*\boldsymbol{b}) + a_4\left(\boldsymbol{b^2} - \tfrac{1}{3}\{\boldsymbol{b^2}\}\boldsymbol{I}\right) = a_1\boldsymbol{S}^* + \boldsymbol{L}^*, \tag{9}$$

where $\boldsymbol{S}^* = \lambda\boldsymbol{S}$, $\boldsymbol{W}^* = \lambda\boldsymbol{W}$ and $\boldsymbol{L}^* = \lambda\boldsymbol{L}$.

It should be noted that the buoyancy effect not only enters as (G/ε) in $1/g$, but also appears in $\boldsymbol{L}$ as a symmetric traceless tensor $\boldsymbol{F}$. Equation (9) gives an implicit algebraic equation for the Reynolds stress anisotropy tensor for a homogeneous, buoyant turbulent flow at equilibrium. Due to the coupling between the velocity and the thermal field shown in (9), knowledge of the turbulent heat flux vector is required. Once the heat flux vector is known, $\boldsymbol{L}^*$ on the right-hand side of (9) can be evaluated. Therefore, (9) and other equations to be derived are used to analyse the equilibrium states of buoyant turbulence.

3. Evolution of the turbulent heat flux vector

For homogeneous buoyant shear flows, the equation governing the transport of $\overline{u_i\theta}$ can be written as

$$\frac{\mathrm{d}(\overline{u_i\theta})}{\mathrm{d}t} = P_{\theta i} + \Phi_{\theta i} + G_{\theta i}, \tag{10}$$

where $P_{\theta i} = -\overline{u_iu_j}(\partial\Theta/\partial x_j) - \overline{u_j\theta}(\partial U_i/\partial x_j)$ is the production of $\overline{u_i\theta}$ due to mean shear and mean temperature gradient, and $G_{\theta i} = -\beta g_i\overline{\theta^2}$ is the buoyant production of $\overline{u_i\theta}$. In order to close (10), the pressure–scrambling and viscous dissipation vector $\Phi_{\theta i}$ (hereafter pressure–scrambling vector for short) requires modelling and is assumed to be (e.g. So & Speziale 1999)

$$\Phi_{\theta i} = -C_{1\theta}\frac{\varepsilon}{k}\overline{u_i\theta} + C_{2\theta}\overline{u_j\theta}\frac{\partial U_i}{\partial x_j} + C_{3\theta}\overline{u_j\theta}\frac{\partial U_j}{\partial x_i} + C_{4\theta}\overline{u_iu_j}\frac{\partial\Theta}{\partial x_j} + C_{5\theta}\beta g_i\overline{\theta^2}, \tag{11}$$

where the values for the $C_{i\theta}$ closure constants will be assigned later.

Just as in the case of b_{ij}, the evolution of $\overline{u_i\theta}$ is analysed by considering a dimensionless form of the heat flux vector equation. Introducing the normalized heat flux vector, $\zeta_i = \overline{u_i\theta}/\sqrt{kk_\theta}$, where $k_\theta = \overline{\theta^2}/2$, the following identity can be written:

$$\frac{\mathrm{d}\zeta_i}{\mathrm{d}t} = \frac{\mathrm{d}}{\mathrm{d}t}\left(\frac{\overline{u_i\theta}}{\sqrt{kk_\theta}}\right) = \frac{1}{\sqrt{kk_\theta}}\frac{\mathrm{d}(\overline{u_i\theta})}{\mathrm{d}t} - \frac{\overline{u_i\theta}}{2\sqrt{kk_\theta}}\left[\frac{1}{k}\frac{\mathrm{d}k}{\mathrm{d}t} + \frac{1}{k_\theta}\frac{\mathrm{d}k_\theta}{\mathrm{d}t}\right]. \tag{12}$$

For the homogeneous case under consideration here, the equations for k and k_θ are given by

$$\frac{\mathrm{d}k}{\mathrm{d}t} = \tilde{P} - \varepsilon + G, \tag{13}$$

$$\frac{\mathrm{d}k_\theta}{\mathrm{d}t} = \tilde{P}_\theta - \varepsilon_\theta, \tag{14}$$

where $\tilde{P}_\theta = -\overline{u_i\theta}\,(\partial\Theta/\partial x_i)$ is the turbulent production of k_θ. Note that these two equations are exact for homogeneous flows; therefore they do not need modelling. Substituting (13) and (14) into (12) then yields,

$$\dot{\zeta}_i = \frac{\mathrm{d}\zeta_i}{\mathrm{d}t} = \frac{1}{\sqrt{kk_\theta}}[P_{\theta i} + \Phi_{\theta i} + G_{\theta i}] - \frac{\zeta_i}{2}\frac{\varepsilon_\theta}{k_\theta}\left[R\left(\frac{\tilde{P}}{\varepsilon} - 1 + \frac{G}{\varepsilon}\right) + \left(\frac{\tilde{P}_\theta}{\varepsilon_\theta} - 1\right)\right], \tag{15}$$

where $R = (k_\theta/\varepsilon_\theta)/(k/\varepsilon)$ is the turbulent time scale ratio. For an equilibrium turbulence field, $\dot{\zeta}_i = 0$, and (15) yields an implicit algebraic equation for the scaled heat flux vector

$$\frac{1}{\varepsilon_\theta}\sqrt{\frac{k_\theta}{k}}[P_{\theta i} + \Phi_{\theta i} + G_{\theta i}] - \frac{\zeta_i}{2}\left[R\left(\frac{\tilde{P}}{\varepsilon} - 1 + \frac{G}{\varepsilon}\right) + \left(\frac{\tilde{P}_\theta}{\varepsilon_\theta} - 1\right)\right] = 0, \tag{16}$$

where the scaled variables $\Theta_i = (k/\varepsilon)\sqrt{k/k_\theta}(\partial\Theta/\partial x_i)$ and $\bar{g}_i = (\sqrt{k_\theta/k})(k/\varepsilon)\beta\, g_i$ have been introduced. Substituting $P_{\theta i}$, $\Phi_{\theta i}$ and $G_{\theta i}$ into (16) leads to the heat flux equation

$$-\frac{1}{2}\left[R\left(\frac{\tilde{P}}{\varepsilon} - 1 + \frac{G}{\varepsilon} + 2C_{1\theta}\right) + \left(\frac{\tilde{P}_\theta}{\varepsilon_\theta} - 1\right)\right]\zeta_i - RC_S\zeta_k S^*_{ki} + RC_\Omega\zeta_k W^*_{ki}$$
$$= \tfrac{2}{3}R(1 - C_{4\theta})\Theta_i + 2R(1 - C_{5\theta})\,\bar{g}_i + 2R(1 - C_{4\theta})\Theta_k b_{ki}, \tag{17}$$

or, in more compact form,

$$-\frac{1}{a_\theta}\zeta_i - RC_S\zeta_k S^*_{ki} + RC_\Omega\zeta_k W^*_{ki} = \tfrac{2}{3}RC_b\Theta_i + 2RC_{\bar{g}}\bar{g}_i + 2RC_b\Theta_k b_{ki}, \tag{18}$$

where

$$\frac{1}{a_\theta} = \frac{1}{2}\left[R\left(\frac{\tilde{P}}{\varepsilon} - 1 + \frac{G}{\varepsilon} + 2C_{1\theta}\right) + \left(\frac{\tilde{P}_\theta}{\varepsilon_\theta} - 1\right)\right], \tag{19}$$

$C_S = 1 - C_{2\theta} - C_{3\theta}$, $C_\Omega = 1 - C_{2\theta} + C_{3\theta}$, $C_{\bar{g}} = 1 - C_{5\theta}$, and $C_b = 1 - C_{4\theta}$. Equation (18) is an implicit algebraic heat flux equation for homogeneous buoyant turbulent flows that is coupled with the corresponding implicit algebraic equation (9) for the Reynolds stress anisotropy tensor through $\boldsymbol{L}^*$.

4. Equivalent scalar representation

For non-buoyant homogeneous turbulence with a two-dimensional mean flow, Jongen & Gatski (1998) have shown that the polynomial tensor representation of the Reynolds stress anisotropy tensor $\boldsymbol{b}$ can be written as

$$\boldsymbol{b} = -\frac{\{\boldsymbol{bS}^*\}}{2\Pi^*_S}\boldsymbol{S}^* + \frac{\{\boldsymbol{bW}^*\boldsymbol{S}^*\}}{4\Pi^*_S\Pi^*_W}(\boldsymbol{S}^*\boldsymbol{W}^* - \boldsymbol{W}^*\boldsymbol{S}^*) + \frac{3}{2}\frac{\{\boldsymbol{bS}^{*\mathbf{2}}\}}{\Pi^{*2}_S}\left(\boldsymbol{S}^{*\mathbf{2}} + \tfrac{2}{3}\Pi^*_S\boldsymbol{I}\right), \tag{20}$$

where $2\Pi^*_S = -\{\boldsymbol{S}^{*\mathbf{2}}\}$ and $2\Pi^*_W = -\{\boldsymbol{W}^{*\mathbf{2}}\}$ define the second invariants of the scaled

strain rate and rotation rate tensors, respectively. The generation of these scalar invariants formed from the anisotropy tensor $\boldsymbol{b}$ and the kinematic tensors $\boldsymbol{S}^*$ and $\boldsymbol{W}^*$ then provides a closed system of three equations in the three unknowns (invariants) $\{\boldsymbol{bS}^*\}, \{\boldsymbol{bW}^*\boldsymbol{S}^*\}, \{\boldsymbol{bS}^{*\mathbf{2}}\}$. This led to the identification of, and relationship between, the known state variables $\tilde{P}/\varepsilon$ and Sk/ε for a range of homogeneous flows. This same methodology can be extended and applied here to the buoyant homogeneous case where the identity of, and relationship between, the equilibrium state variables has not been previously determined.

Since the coupling between the turbulent velocity and thermal field in (9) is through the tensor $\boldsymbol{L}^*$ containing the buoyancy terms, the starting point for the buoyant case is again the formation of the equations for the three invariants $\{\boldsymbol{bS}^*\}, \{\boldsymbol{bW}^*\boldsymbol{S}^*\}, \{\boldsymbol{bS}^{*\mathbf{2}}\}$ from (9). These are given by (Jongen & Gatski 1998),

$$\frac{1}{g}\{\boldsymbol{bS}^*\} + 2a_3\{\boldsymbol{bS}^{*\mathbf{2}}\} - 2a_2\{\boldsymbol{bW}^*\boldsymbol{S}^*\} + \frac{a_4}{\Pi_S^*}\{\boldsymbol{bS}^*\}\{\boldsymbol{bS}^{*\mathbf{2}}\} = 2a_1\Pi_S^* - L_1^*, \tag{21}$$

$$\frac{1}{g}\{\boldsymbol{bW}^*\boldsymbol{S}^*\} - 2a_2\Pi_S^*\mathscr{R}^2\{\boldsymbol{bS}^*\} + \frac{a_4}{\Pi_S^*}\{\boldsymbol{bW}^*\boldsymbol{S}^*\}\{\boldsymbol{bS}^{*\mathbf{2}}\} = -L_2^*, \tag{22}$$

$$\frac{1}{g}\{\boldsymbol{bS}^{*\mathbf{2}}\} - \tfrac{2}{3}a_3\Pi_S^*\{\boldsymbol{bS}^*\} - \frac{a_4}{6}\{\boldsymbol{bS}^*\}^2 + \frac{a_4}{6\Pi_S^*\mathscr{R}^2}\{\boldsymbol{bW}^*\boldsymbol{S}^*\}^2 - \frac{a_4}{2\Pi_S^*}\{\boldsymbol{bS}^{*\mathbf{2}}\}^2 = -L_3^*, \tag{23}$$

where $\mathscr{R}^2$ $(= -\Pi_W^*/\Pi_S^*)$ is a flow parameter (e.g. $\mathscr{R}^2 = 1$ for a pure shear flow and $\mathscr{R}^2 = 0$ for a plane strain flow). As (21)–(23) show, the coupling with the thermal field occurs through the invariants $L_1^* = \{\boldsymbol{L}^*\boldsymbol{S}^*\}$, $L_2^* = \{\boldsymbol{L}^*\boldsymbol{W}^*\boldsymbol{S}^*\}$, and $L_3^* = \{\boldsymbol{L}^*\boldsymbol{S}^{*\mathbf{2}}\}$. Unfortunately, unlike the non-buoyant case, where the right-hand sides of (21)–(23) were known, buoyancy effects are not only reflected implicitly in $\boldsymbol{b}$ (through g), but also explicitly in L_1^*, L_2^*, and L_3^* as

$$L_1^* = \{\boldsymbol{L}^*\boldsymbol{S}^*\} = a_6\left(\frac{G}{\varepsilon}\right)\{\boldsymbol{FS}^*\} = -a_6\left[\bar{g}_i\zeta_j S_{ji}^*\right] = -a_6 L_1, \tag{24a}$$

$$L_2^* = \{\boldsymbol{L}^*\boldsymbol{W}^*\boldsymbol{S}^*\} = a_6\left(\frac{G}{\varepsilon}\right)\{\boldsymbol{FW}^*\boldsymbol{S}^*\} = -a_6\left[\bar{g}_i\zeta_j W_{jk}^* S_{ki}^*\right] = -a_6 L_2, \tag{24b}$$

$$L_3^* = \{\boldsymbol{L}^*\boldsymbol{S}^{*2}\} = a_6\left(\frac{G}{\varepsilon}\right)\{\boldsymbol{FS}^{*2}\} = \tfrac{2}{3}a_6\Pi_S^*\left(\frac{G}{\varepsilon}\right) + a_6\Pi_S^*\left[\bar{g}_i\zeta_k\delta_{ki}^{(2d)}\right] \tag{24c}$$

where, from the Cayley–Hamilton Theorem for two-dimensional mean flows, $S_{jk}^*W_{ki}^* = -W_{jk}^*S_{ki}^*$ has been used. The present focus is solely on the coupling effects of the heat flux vector. For this reason, effects of dissipation rate anisotropy have not been included ($\boldsymbol{d} = 0$) in the present formulation. While it is also possible to proceed with the analysis including the contribution of the nonlinear term ($\boldsymbol{b}^2 - \{\boldsymbol{b}^2\}\boldsymbol{I}/3$), the added complexity is not justified for the case of homogeneous turbulence under study here.

The writing of (24*a–c*) is in anticipation of a later comparison with DNS data of buoyant pure shear flows where the mean shear gradient makes an arbitrary angle φ with the (x_1, x_3)-plane (Jacobitz & Sarkar 1998). It should be pointed out that the present analysis is carried out for two-dimensional mean flow only. Thus, equations (24*a–c*) are only applicable for cases where $\varphi = 0$ and $\varphi = \pi/2$. Therefore, in writing (24*a–c*), $\delta_{ij}^{(2d)}$ is used to represent the two cases where $\varphi = 0$ and $\varphi = \pi/2$.

For the $\varphi = 0$ case, $\delta_{ij}^{(2d)} = 1$ for $i = j = 1$ or 3, and 0 for $i = j = 2$ or $i \neq j$, while, for the $\varphi = \pi/2$ case, $\delta_{ij}^{(2d)} = 1$ for $i = j = 1$ or 2, and 0 for $i = j = 3$ or $i \neq j$.

For the two cases of φ considered here, the mean velocity field in these homogeneous flows can be described in an appropriate reference frame for pure shear and pure strain, respectively, by the expressions

$$\frac{\partial U_i}{\partial x_j} = S\cos\varphi\,\delta_{i1}\delta_{j3} + S\sin\varphi\,\delta_{i1}\delta_{j2}, \tag{25a}$$

$$\frac{\partial U_i}{\partial x_j} = [-S\,\delta_{i1}\delta_{j1} + S\,\delta_{i3}\delta_{j3}], \tag{25b}$$

and the thermal field by the expression

$$\frac{\partial \Theta}{\partial x_i} = \left(0, 0, \frac{\partial \Theta}{\partial x_3}\right), \tag{26}$$

where $S/2$ is the strain rate (Leuchter & Benoit 1991), and Θ is the mean temperature. As seen, the distortion is in the (x_1, x_3)-plane with the normalized gravitational acceleration given by $\bar{g}_i = (0, 0, \bar{g}_3)$, where $\bar{g}_3 = (\sqrt{k_\theta/k})\,(k/\varepsilon)\beta\, g_3 = -(\sqrt{k_\theta/k})(k/\varepsilon)\beta\, g_c$, and with the relevant mean temperature gradient aligned with the gravitational vector. For such flows, two components of the heat flux exist, i.e. $\overline{u_1\theta}$ and $\overline{u_3\theta}$ (or ζ_1 and ζ_3 in scaled variables). In the Appendix, a closed system of seven equations in seven unknown variables is derived for the case of two-dimensional mean flows.

This system can be further reduced by eliminating the explicit dependence on both $\{\boldsymbol{bW^*S^*}\}$ and $\{\boldsymbol{bS^{*2}}\}$. The ratio $\tilde{P}/\varepsilon (= -2\{\boldsymbol{bS^*}\})$ then satisfies the equation

$$\left[1 + 4\Pi_S^* g^2\left(\frac{a_3^2}{3} - a_2^2\mathscr{R}^2\right)\right]\left(\frac{\tilde{P}}{\varepsilon}\right) = -4g\left[a_1\Pi_S^* + \frac{a_6}{2}\left(L_1 + 2a_2 g L_2 + \tfrac{4}{3}a_3 g\Pi_S^*\left(\frac{G}{\varepsilon}\right) + 2a_3 g\Pi_S^*\left[\bar{g}_3\zeta_k\delta_{k3}^{(2d)}\right]\right)\right]. \tag{27}$$

In the non-buoyant ($\beta = L_1 = L_2 = G/\varepsilon = 0$) homogeneous turbulence case, (27) was sufficient for closure and the state variable $\tilde{P}/\varepsilon$ satisfied a cubic equation (e.g. Jongen & Gatski 1998).

In the buoyant case, in order to close (27), it is necessary to determine the invariants $[\bar{g}_3\zeta_k S_{k3}^*]$, $[\bar{g}_3\zeta_k W_{kl}^* S_{l3}^*]$ and G/ε $(= -\bar{g}_3\zeta_3)$. A general derivation of the corresponding invariant equations is presented in the Appendix. However, they can be simplified by eliminating $\{\boldsymbol{bW^*S^*}\}$ and $\{\boldsymbol{bS^{*2}}\}$ from (A 4)–(A 7). The general two-dimensional equations (for the $\varphi = 0$ and $\pi/2$ case) necessary for determining $L_1 (= [\bar{g}_3\zeta_j S_{j3}^*])$, $L_2 (= [\bar{g}_3\zeta_j W_{jk}^* S_{k3}^*])$ and (G/ε) are

$$-\frac{1}{a_\theta}L_1 + R\left(C_\Omega + \frac{a_6 g C_b}{\Pi_S^*\mathscr{R}^2}\left[\bar{g}_3\Theta_k W_{k3}^*\right]\right)L_2 + R\left\{C_S\Pi_S^* - C_b a_6 g\left[\bar{g}_3\Theta_k S_{k3}^*\right]\right\}\left[\bar{g}_3\zeta_k\delta_{k3}^{(2d)}\right]$$

$$-\tfrac{2}{3}RC_b a_6 g\left[\bar{g}_3\Theta_k S_{k3}^*\right]\left(\frac{G}{\varepsilon}\right) = \tfrac{1}{3}RC_b\left[2 + a_3 g\left(\frac{\tilde{P}}{\varepsilon}\right)\right]\left[\bar{g}_3\Theta_k S_{k3}^*\right] + 2RC_{\bar{g}}\left[\bar{g}_3^2 S_{33}^*\right]$$

$$-\tfrac{1}{2}RC_b\left(\frac{\tilde{P}}{\varepsilon}\right)\left[\bar{g}_3\Theta_k\delta_{k3}^{(2d)}\right] + a_2 g RC_b\left(\frac{\tilde{P}}{\varepsilon}\right)\left[\bar{g}_3\Theta_k W_{k3}^*\right], \tag{28}$$

$$RC_\Omega \Pi_S^* \mathscr{R}^2 L_1 - \left(\frac{1}{a_\theta} + a_6 g RC_b \left[\bar{g}_3 \Theta_k \delta_{k3}^{(2d)}\right]\right) L_2 - a_6 g RC_b \left[\bar{g}_3 \Theta_k W_{kl}^* S_{l3}^*\right]$$

$$\times \left(\left[\bar{g}_3 \zeta_k \delta_{k3}^{(2d)}\right] + \frac{2}{3}\frac{G}{\varepsilon}\right) - RC_S \Pi_S^* \left[\bar{g}_3 \zeta_k W_{k3}^*\right] = \tfrac{1}{3} RC_b \left[2 + a_3 g \left(\frac{\tilde{P}}{\varepsilon}\right)\right] \left[\bar{g}_3 \Theta_k W_{kl}^* S_{l3}^*\right]$$

$$+ 2RC_{\bar{g}} \left[\bar{g}_3^2 W_{3k}^* S_{k3}^*\right] + \tfrac{1}{2} RC_b \left(\frac{\tilde{P}}{\varepsilon}\right) \left[\bar{g}_3 \Theta_k W_{k3}^*\right] - a_2 g RC_b \Pi_S^* \mathscr{R}^2 \left(\frac{\tilde{P}}{\varepsilon}\right) \left[\bar{g}_3 \Theta_k \delta_{k3}^{(2d)}\right], \tag{29}$$

$$R\left(C_S + \frac{a_6 g C_b}{\Pi_S^*} \left[\bar{g}_3 \Theta_k S_{k3}^*\right]\right) L_2 + R\left\{C_\Omega \Pi_S^* \mathscr{R}^2 - a_6 g C_b \left[\bar{g}_3 \Theta_k W_{k3}^*\right]\right\} \left[\bar{g}_3 \zeta_k \delta_{k3}^{(2d)}\right]$$

$$- \tfrac{2}{3} RC_b a_6 g \left[\bar{g}_3 \Theta_k W_{k3}^*\right] \left(\frac{G}{\varepsilon}\right) - \frac{1}{a_\theta} \left[\bar{g}_3 \zeta_k W_{k3}^*\right] = \tfrac{1}{3} RC_b \left[2 + a_3 g \left(\frac{\tilde{P}}{\varepsilon}\right)\right] \left[\bar{g}_3 \Theta_k W_{k3}^*\right]$$

$$+ \frac{RC_b}{2\Pi_S^*} \left(\frac{\tilde{P}}{\varepsilon}\right) \left[\bar{g}_3 \Theta_k S_{kl}^* W_{l3}^*\right] + a_2 g RC_b \mathscr{R}^2 \left(\frac{\tilde{P}}{\varepsilon}\right) \left[\bar{g}_3 \Theta_k S_{k3}^*\right], \tag{30}$$

$$-RC_S L_1 - \frac{a_6 g}{\Pi_S^{*2} \mathscr{R}^2} RC_b \left[\bar{g}_3 \Theta_k W_{kl}^* S_{l3}^*\right] L_2 + a_6 g RC_b \left\{2\left[\bar{g}_3 \Theta_3\right] - 3\left[\bar{g}_3 \Theta_k \delta_{k3}^{(2d)}\right]\right\} \left[\bar{g}_3 \zeta_k \delta_{k3}^{(2d)}\right]$$

$$+ RC_\Omega \left[\bar{g}_3 \zeta_k W_{k3}^*\right] + \left(\frac{1}{a_\theta} + \tfrac{4}{3} a_6 g RC_b \left[\bar{g}_3 \Theta_3\right] - 2a_6 g RC_b \left[\bar{g}_3 \Theta_k \delta_{k3}^{(2d)}\right]\right) \left(\frac{G}{\varepsilon}\right)$$

$$= \tfrac{1}{3} RC_b \left[2 - 2a_3 g \left(\frac{\tilde{P}}{\varepsilon}\right)\right] \left[\bar{g}_3 \Theta_3\right] + 2RC_{\bar{g}} \bar{g}_3^2 + \frac{RC_b}{2\Pi_S^*} \left(\frac{\tilde{P}}{\varepsilon}\right) \left[\bar{g}_3 \Theta_k S_{k3}^*\right]$$

$$- \frac{a_2 g}{\Pi_S^*} RC_b \left(\frac{\tilde{P}}{\varepsilon}\right) \left[\bar{g}_3 \Theta_k W_{kl}^* S_{l3}^*\right] + a_3 g RC_b \left(\frac{\tilde{P}}{\varepsilon}\right) \left[\bar{g}_3 \Theta_k \delta_{k3}^{(2d)}\right]. \tag{31}$$

The explicit dependence on the scalar $[\bar{g}_3 \zeta_k W_{k3}^*]$ can be eliminated from (28)–(31); however, the resulting forms of these equations would be sufficiently complex to warrant retaining the equation for $[\bar{g}_3 \zeta_k W_{k3}^*]$ given by (30). In addition, (28)–(31) are not independent equations and can be related to one another through factors involving the components of the strain rate and rotation rate tensors. As will be seen shortly, the exact relationship is dependent on the particular flow under investigation.

Up to this point in the analysis, (27)–(31) provide a set of five equations for the five unknowns $(\tilde{P}/\varepsilon)$, L_1, L_2, $[\bar{g}_3 \zeta_k W_{k3}^*]$, and (G/ε), respectively. It should be recognized that in these equations the time scale ratio R and the flow parameter $\mathscr{R}^2$ appear as parameters and are assumed known ($\boldsymbol{S}^*$ and $\boldsymbol{W}^*$ known). For a given two-dimensional mean flow, the associated turbulent velocity and thermal field time scales are obtained from the k, ε, k_θ and ε_θ equations at equilibrium ($\dot{b}_{ij} = 0$, $\dot{\zeta}_i = 0$).

Since a_θ retains a functional dependence on the thermal production-to-dissipation rate ratio $\tilde{P}_\theta/\varepsilon_\theta$ $(= -R\,\zeta_i \Theta_i)$, it is necessary to obtain an independent relation for this ratio. This relation can be obtained from the evolution equations for k and k_θ, given in (13) and (14), by constructing a corresponding non-dimensional evolution

equation for the ratio k/k_θ,

$$\left(\frac{k}{k_\theta}\right)\frac{\mathrm{d}(k_\theta/k)}{\mathrm{d}t^*} = \frac{1}{S^*R}\left[\left(\frac{\tilde{P}_\theta}{\varepsilon_\theta}-1\right)-R\left(\frac{\tilde{P}}{\varepsilon}-1+\frac{G}{\varepsilon}\right)\right], \tag{32}$$

where the non-dimensional time $t^* = St$. At the fixed points ($\dot{b}_{ij} = 0$, $\dot{\zeta}_i = 0$), equilibrium values exist for all the terms on the right-hand side of (32). Thus, the ratio k_θ/k is characterized by the right-hand side of (32) and could exhibit, in general, exponential growth or decay or a fixed-point equilibrium state. If equilibrium is reached by k_θ/k, then this state is characterized by the vanishing of the right-hand side of (32) which then provides a relation for $\tilde{P}_\theta/\varepsilon_\theta$ in terms of the other state variables:

$$\frac{\tilde{P}_\theta}{\varepsilon_\theta} = 1 + R\left(\frac{\tilde{P}}{\varepsilon}-1+\frac{G}{\varepsilon}\right). \tag{33}$$

A consequence of (33) is that the closure coefficient a_θ, given by (19), is now simply

$$\frac{1}{a_\theta} = R\left[\frac{\tilde{P}}{\varepsilon}-1+\frac{G}{\varepsilon}+C_{1\theta}\right], \tag{34}$$

a result which underscores the importance of the closure coefficient $C_{1\theta}$ in describing the behaviour of the thermal field. In addition, from (16) it is apparent that the fixed point for the scaled heat flux vector ζ_i is only dependent on the heat flux equation (10) with no influence from either the k or k_θ equation, i.e. (13) or (14). This is further reflected in an examination of (28)–(31). Using (34) in these equations results in the disappearance of the time scale variable R from the equations. Thus, the equilibrium state achieved by the heat flux vector is independent of the behaviour of the thermal time scale $k_\theta/\varepsilon_\theta$, whereas the ratio $\tilde{P}_\theta/\varepsilon_\theta$ retains the dependence on R as well as on the turbulent velocity and heat flux fields.

This observation is consistent with the generalized linearity principle proposed by Pope (1983) for modelling scalars in turbulent flows. However, most models employ either the mixed time scale given by k/ε and $k_\theta/\varepsilon_\theta$ (e.g. Youssef, Nagano & Tagawa 1992; So & Speziale 1999) or the time scale ratio R in the empirical constants of the ε_θ-equation (e.g. Jones & Musonge 1988; Craft & Launder 1989; Nagano & Shimada 1996). For the first time, the present analysis shows that R simply does not appear in the heat flux equations, only in the $\tilde{P}_\theta/\varepsilon_\theta$ equation. Thus the use of R to model the heat flux vector might not be totally appropriate even though it gives enough good results to justify its adoption. Even though the presence of R does not change the dimension of the model, nevertheless it violates the linearity principle.

In the next section, the behaviour of these variables that characterize the equilibrium state associated with $\dot{b}_{ij} = \dot{\zeta}_i = 0$ is examined for specific mean velocity and thermal fields.

5. Equilibrium states in buoyant homogeneous flows

In general, it is not possible to obtain a closed analytic solution of (27)–(31), and a numerical solution of the coupled set of nonlinear algebraic equations is required. Nevertheless, even these nonlinear algebraic equations are more amenable to analysis in the specific cases that will now be examined. The cases to be examined are those with $\varphi = 0$. Only equations relating to pure shear flow, plane strain flow and uniform

flow are given. The relevant equations for other values of φ will be given when the specific case is considered.

5.1. *Turbulent velocity and thermal field closure constants*

It is important to recognize that up to this point specific closure constants have not been assigned to the rather general functional forms that have been assumed to close both the turbulent Reynolds stress and heat flux equations. The equilibrium state assumed here should exactly correspond to the long-time numerical solution of the evolution equations given by (1), (10), (13), and (14) coupled with the corresponding modelled equations for ε and ε_θ (see Zhao *et al.* 2001). These equations and closure constants to be specified are designated as the SSG/AD model from here on for easy reference. This model is used to perform the numerical calculations to verify the solutions of the respective algebraic equations for the different specific cases considered below.

For the Reynolds stress transport equation (1), a linearized form of the SSG pressure–strain rate model (Speziale *et al.* 1991) as given in (2) is assumed for Π_{ij}. The associated constants are specified as $C_1^0 = 3.4$, $C_1^1 = 1.8$, $C_2 = 0.36$, $C_3 = 1.25$, $C_4 = 0.4$, $C_5 = 0$ and $C_6 = 0.3$. Closure for the dissipation rate is also required, and as pointed out earlier, the dissipation rate anisotropy is assumed to be zero here. The isotropic dissipation rate equation used is given by (see Zhao *et al.* 2001 for details),

$$\frac{\mathrm{d}\varepsilon}{\mathrm{d}t} = \left(\frac{\varepsilon^2}{k}\right)\left[C_{\varepsilon 1}\left(\frac{\tilde{P}}{\varepsilon}\right) - \left(C_{\varepsilon 2} - 2C_{\varepsilon 4}S^*\right) - C_{\varepsilon 3}\left(\frac{G}{\varepsilon}\right)\right], \tag{35}$$

with closure coefficients $C_{\varepsilon 1} = 1.44$, $C_{\varepsilon 2} = 1.83$, $C_{\varepsilon 3} = 1.44$, $C_{\varepsilon 4} = 0.042$.

The scalar heat flux equation (10) contains the pressure–scrambling vector $\Phi_{\theta i}$. The modelling of this term closely parallels that of Π_{ij}, in that the model is partitioned into three parts, a slow part, $\Phi_{\theta i}^{(S)}$, a rapid part, $\Phi_{\theta i}^{(R)}$, and a buoyant part, $\Phi_{\theta i}^{(B)}$. Monin (1965) proposed a model for the slow part similar to the linear 'return-to-isotropy' model for the slow part of Π_{ij}. This is given by the first term on the right-hand side of (11) with corresponding closure coefficient $C_{1\theta}$. The rapid part can be written in general form as $\Phi_{\theta i}^{(R)} = b_{ik}^m\,(\partial U_k/\partial x_m)$ with different models proposed for b_{ik}^m. Finally, the buoyant part was modelled by assuming it to be proportional to k_θ and that is given by the last term on the right-hand side of (11). If b_{ik}^m is assumed to be linear in the heat fluxes (Lumley 1978), a simple expansion of b_{ik}^m in terms of the heat flux would lead to the second and third terms on the right-hand side of (11). The fourth term on the right-hand side of (11) was proposed by Shabany & Durbin (1997) in order to account for the interaction of the turbulence and the mean thermal field. A more elaborate model for b_{ik}^m has been derived by Craft & Launder (1989) and it includes quadratic terms in b_{ij} and interaction terms between b_{ij} and ζ_i. The coefficients $C_{2\theta} = 0.8$ and $C_{3\theta} = -0.2$ were proposed by Launder (1973) and Lumley (1978). Later, $C_{2\theta} = 0.4$ and $C_{3\theta} = 0.33$ were found to give better results by Launder (1988). Since then, most studies have assumed an absolute value of 0.5 for $C_{2\theta}$ and $C_{3\theta}$. However, in a model evaluation analysis carried out by Wikstrom, Wallin & Johansson (2000) against DNS data of homogeneous shear flows with a mean temperature gradient imposed either in the streamwise, transverse or spanwise direction, they found that the presence of the $C_{3\theta}$ term in (11) led to erroneous results in the prediction of the streamwise to transverse heat flux ratio. In their calculations, the $C_{4\theta}$ term was set to zero. Furthermore, they found that reasonable results can also be obtained when $C_{2\theta}$ and $C_{3\theta}$ are set to zero while $C_{1\theta} = 2.5$ and $C_{4\theta} = 0.35$ were specified instead. Therefore, their investigation showed that $C_{3\theta}$ should be zero if

reasonable results were to be predicted for non-isothermal, homogeneous shear flows. As will be shown shortly, the result $C_{3\theta} = 0$ can also be obtained rigorously from the current formulation by examining the limiting case of non-isothermal shear flow where Richardson number $Ri = 0$. In this study, the closure constants used for the model of $\Phi_{\theta i}$ are assumed to take the values $C_{1\theta} = 3.28$, $C_{2\theta} = 0.40$, $C_{3\theta} = C_{4\theta} = 0$ and $C_{5\theta} = C_{2\theta}$ (Launder 1978; So & Speziale 1999; Wikstrom *et al.* 2000).

Finally, the ε_θ equation required for the solution of the k_θ equation can be written as (see Zhao *et al.* 2001 for details)

$$\frac{\mathrm{d}\varepsilon_\theta}{\mathrm{d}t} = \frac{1}{2}\left(\frac{\varepsilon_\theta^2}{k_\theta}\right)\left[(C_{d1} + 2C_{d2}R)\left(\frac{\tilde{P}_\theta}{\varepsilon}\right) + 2C_{d3}R\left(\frac{\tilde{P}}{\varepsilon}\right) - (C_{d4} + 2RC_{d5})\right], \tag{36}$$

with closure coefficients given by $C_{d1} = 0$, $C_{d2} = 1.70$, $C_{d3} = 1.40$, $C_{d4} = 2.0$, and $C_{d5} = 0.52$. These are the model constants proposed by Jones & Musonge (1988).

Equations (1), (10), (13), (14), (35) and (36) with the assumed model constants constitute the SSG/AD model used by Zhao *et al.* (2001) in their assessment of a wide range of closure models for buoyant shear flows. The SSG/AD model was shown to be the most appropriate for buoyant shear flows among all closure models examined. This closure model is used to numerically determine the equilibrium parameters for the different buoyant cases and the results are compared with the present analytical predictions assuming the same model constants. In addition, comparisons are also made with DNS data whenever available.

5.2. *Buoyant shear flow*

The case of a uniform shear flow with an imposed mean temperature gradient is one of the simplest shear flows yet one of the most important for both model development and physical insight into buoyant flows. For this case where $\mathscr{R}^2 = 1$, the scaled strain rate S^* and rotation rate W^* are equal, and the only imposed (scaled) mean temperature gradient is $\Theta_i = \Theta_3$. The corresponding Richardson number Ri is then defined as

$$Ri \equiv -\beta g_3 \left(\frac{\partial \Theta}{\partial x_3}\right)\left(\frac{\partial U_1}{\partial x_3}\right)^{-2} = -\frac{\bar{g}_3 \Theta_3}{S^{*2}}, \tag{37}$$

where scaled variables have been introduced. Using these relations, (27)–(31) can be reduced to a closed system of three coupled, nonlinear algebraic equations. Equation (27) for the ratio $\left(\tilde{P}/\varepsilon\right)$ becomes

$$\left[1 + g^2 S^{*2}\left(a_2^2 - \frac{a_3^2}{3}\right)\right]\left(\frac{\tilde{P}}{\varepsilon}\right) - a_6 g S^*\left[\left(\frac{G_{13}}{\varepsilon}\right) - gS^*\left(a_2 + \frac{a_3}{3}\right)\left(\frac{G}{\varepsilon}\right)\right] = a_1 g S^{*2}, \tag{38}$$

where $L_1 = -G_{13}S^*/2\varepsilon$ and $L_2 = GS^{*2}/4\varepsilon$ have been used. The algebraic equations needed to describe the behaviour of the ratios $G_{13}/\varepsilon(= -\bar{g}_3\zeta_1)$ and $G/\varepsilon(= -\bar{g}_3\zeta_3)$ can be derived from (28)–(31) and are given by

$$-2S^* C_b\left(\frac{\tilde{P}}{\varepsilon}\right) Ri + 2\left(\frac{\tilde{P}}{\varepsilon} - 1 + \frac{G}{\varepsilon} + C_{1\theta}\right)\left(\frac{G_{13}}{\varepsilon}\right) + S^*(C_S + C_\Omega)\left(\frac{G}{\varepsilon}\right) = 0, \tag{39}$$

$$2gS^{*2}C_b\,(a_3 - 3a_2)\left(\frac{\tilde{P}}{\varepsilon}\right) Ri + 3S^*(C_S - C_\Omega)\left(\frac{G_{13}}{\varepsilon}\right)$$
$$+6\left(\frac{\tilde{P}}{\varepsilon} - 1 + \frac{G}{\varepsilon} + C_{1\theta} - \tfrac{4}{3}a_6 g S^{*2} C_b Ri\right)\left(\frac{G}{\varepsilon}\right) = -4S^{*2}C_b Ri + 12C_{\bar{g}}\bar{g}_3^2. \quad (40)$$

Equations (38)–(40) are now a closed set of nonlinear, algebraic equations. The solution to these equations yields the equilibrium values for $\tilde{P}/\varepsilon$, G_{13}/ε and G/ε in terms of the corresponding values for S^*, $\bar{g}_3$ (or Θ_3) and Ri. These results, when coupled with a given value of R, then determine the corresponding equilibrium value for $\tilde{P}_\theta/\varepsilon_\theta$ from (33).

In order to verify the existence of the fixed points $\dot{b}_{ij} = 0$ and $\dot{\zeta}_i = 0$ assumed here, the evolution equations of the SSG/AD model, i.e. (1), (10), (13), (14), (35) and (36), are solved. The long-time solution of these equations should yield the same results as those determined here from the fixed-point analysis. Calculations have been carried out for different values of Ri using the initial conditions and scaling outlined in Gerz *et al.* (1989). These are given here as: $(k_o)^n = 4.054 \times 10^{-4}$, $(\varepsilon_o)^n = 1.042 \times 10^{-4}$, $(\overline{u_i u_j})_o^n = 2(k_o)^n/3 = 2.703 \times 10^{-4}$ for $i = j$ and 0 for $i \neq j$, $(\overline{u_i\theta})_o^n = 0$, $(k_\theta)_o^n = 1.352 \times 10^{-4}$, $(\varepsilon_\theta)_o^n = (2/RePr)\,\overline{(\partial\theta/\partial x_j)(\partial\theta/\partial x_j)} = 0.139 \times 10^{-4}$ for $Pr = 5$ (Pr is the molecular Prandtl number and Re is the Reynolds number defined with respect to the mean bulk velocity U_m and L). The superscript n denotes quantities normalized using ΔU, $\Delta\Theta$ and L such that $\Delta U = (\mathrm{d}U/\mathrm{d}x_3)L$ and $\Delta\Theta = (\mathrm{d}\Theta/\mathrm{d}x_3)L$. Thus, the normalized velocity gradient S and the normalized temperature gradient are unity. The subscript o denotes initial condition. Details of the numerical solutions are given in Zhao *et al.* (2001). The long-time numerical solutions yield the state variables $\tilde{P}/\varepsilon$, $\tilde{P}_\theta/\varepsilon_\theta$, G_{13}/ε, G/ε, S^*, and R. If the $\dot{b}_{ij} = 0$ and $\dot{\zeta}_i = 0$ fixed points exist, then these state variables must satisfy (33), (38), (39) and (40) identically. Calculations were carried out for $Ri = 0$ to $Ri \approx 2$ and comparisons between numerical and analytical results are made in this range of Ri.

Figures 1(*a*) to 1(*d*) show the variation of the state variables $\left(\tilde{P}/\varepsilon\right)$, $\left(\tilde{P}_\theta/\varepsilon_\theta\right)$, (G_{13}/ε), and $-(G/\varepsilon)$, respectively, with Ri at equilibrium. Also included on each plot are the corresponding numerical solutions deduced from SSG/AD. The SSG/AD solutions yield the same results as the equilibrium equations for the range of Ri examined. This confirms the consistency of the set of algebraic equations for predicting such homogeneous flows. The plots in figure 1 are made versus Ri, which is a global parameter that depends on imposed conditions rather than on the local state of the turbulence. According to Ivey & Imberger (1991), a turbulent Froude number, Fr_t, based on local properties of the turbulence would be a better parameter to use. Therefore, the variation of the equilibrium values of the different components of b_{ij} is plotted versus Ri and $L_o/(k^{3/2}/\varepsilon) = Fr_t^{3/2}[L_E/(k^{3/2}/\varepsilon)]$ in figures 2(*a*) and 2(*b*), respectively. Here, $L_o = (\varepsilon/N^3)^{1/2}$ is the Ozmidov, or buoyancy, length scale, $L_E = [\beta\,(\partial\Theta/\partial z)]^{-1}$ is the Ellison, or turbulence, length scale, and N is the Brunt–Väisälä frequency defined as $N = \sqrt{|\bar{g}_3\Theta_3|/\lambda^2}$. The behaviour of $|b_{ij}|$ follows the trend of increasing (or decreasing) for small Ri, reaching a maximum (or minimum) at $Ri = 0.2$ and then slowly decreasing (or increasing) to fairly constant values as Ri increases (figure 2*a*). The trend of an initial increasing value of b_{11} and $|b_{33}|$ and a corresponding decreasing value of $|b_{22}|$ and $|b_{13}|$ is supported by the recent DNS data of Jacobitz & Sarkar (1998), who have calculated the behaviour of b_{ij} up to $Ri = 0.2$. Using (37), the normalized L_o can be written as $L_o/(k^{3/2}/\varepsilon) = (\varepsilon/Sk)^{3/2}/Ri^{3/4}$, which indicates that as Ri decreases $L_o/(k^{3/2}/\varepsilon)$ increases and when Ri goes to zero

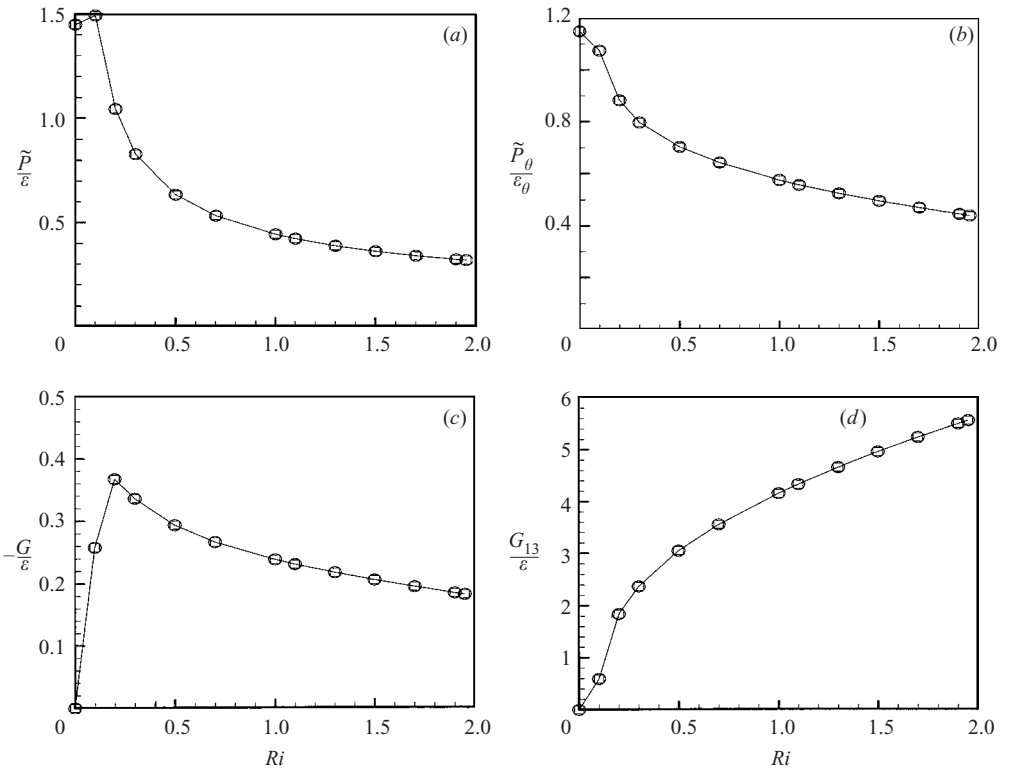

FIGURE 1. Equilibrium state variation of (*a*) $\tilde{P}/\varepsilon$, (*b*) $\tilde{P}_\theta/\varepsilon_\theta$, (*c*) G_{13}/ε, and (*d*) $-(G/\varepsilon)$ with Ri for buoyant shear flows: —□—, SSG/AD model solution; —○—, analytical solution.

$L_o/(k^{3/2}/\varepsilon)$ will go to infinity. The trend of b_{ij} versus $L_o/(k^{3/2}/\varepsilon)$ is much like that shown in figure 2(*a*). In other words, for equilibrium states, either Ri or $L_o/(k^{3/2}/\varepsilon)$ can be used to characterize the behaviour of b_{ij} in buoyant shear flows.

An alternative use of (33) and (38)–(40) is to verify the consistency of the turbulence closure models. One example deals with the form of the model assumed for the pressure–scrambling vector given in (11). For the limiting case of non-isothermal shear flow ($Ri = 0$), the thermal field is decoupled from the velocity field; then (38)–(40) can be rewritten as

$$\left[1 + g^2 S^{*2}\left(a_2^2 - \tfrac{1}{3}a_3^2\right)\right]\left(\frac{\tilde{P}}{\varepsilon}\right) = g a_1 S^{*2}, \tag{41}$$

$$2C_b\Theta_3\left(\frac{\tilde{P}}{\varepsilon}\right) - 2S^*\left(\frac{\tilde{P}}{\varepsilon} - 1 + C_{1\theta}\right)\zeta_1 - S^{*2}(C_S + C_\Omega)\,\zeta_3 = 0, \tag{42}$$

$$2gC_b\Theta_3(a_3 - 3a_2)\left(\frac{\tilde{P}}{\varepsilon}\right) + 3S^*(C_S - C_\Omega)\zeta_1 + 6\left(\frac{\tilde{P}}{\varepsilon} - 1 + C_{1\theta}\right)\zeta_3 = -4C_b\Theta_3. \tag{43}$$

Equation (41) is simply the non-buoyant homogeneous shear flow result (cf. Jongen & Gatski 1998) that correctly reflects the decoupling from the thermal field. In the absence of any mean temperature gradient $\Theta_3 = 0$, (42) and (43) yield the equilibrium

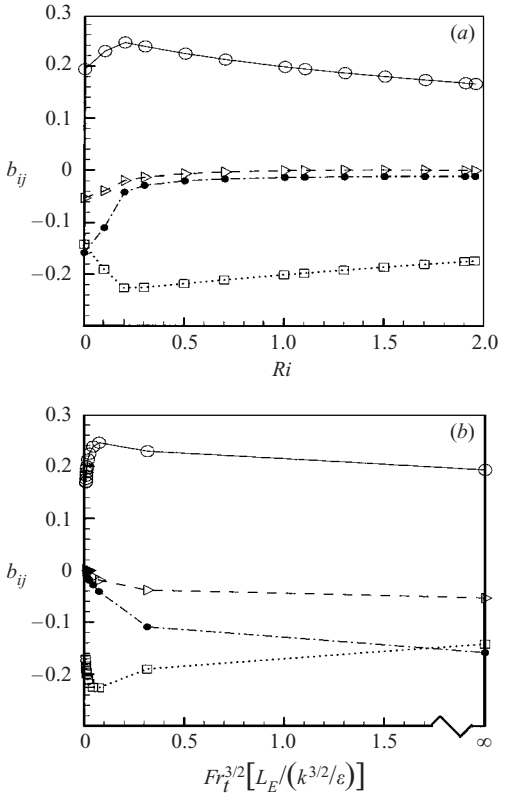

FIGURE 2. Equilibrium-state variation of b_{ij} with: (*a*) Ri and (*b*) $Fr_t^{3/2}[L_E/(k^{3/2}/\varepsilon)]$ for buoyant shear flows: ○, b_{11}; ▷, b_{22}; ●, b_{13}; □, b_{33}.

solution

$$\left\{4\left(\frac{\tilde{P}}{\varepsilon}-1+C_{1\theta}\right)^2+[S^*(C_S-C_\Omega)]^2\right\}\zeta_i=0,\quad i=1,\,3. \tag{44}$$

Since $C_S < C_\Omega$ because $C_S = 1-C_{2\theta}-C_{3\theta}$ and $C_\Omega = 1-C_{2\theta}+C_{3\theta}$, then (44) suggests that $C_S = C_\Omega$ or $C_{3\theta} = 0$ for the (vanishing) heat flux vector to have the correct long-time asymptotic behaviour. For the choice $C_{3\theta} = 0$ with $C_{5\theta} = C_{2\theta}$, $C_{\bar{g}} = C_S = C_\Omega$ and the closure of the pressure–scrambling term in (11) reduces to a calibration of the closure coefficients $C_{1\theta}$, $C_{2\theta}$ and $C_{4\theta}$.

Another example, where the equilibrium equations can be useful in closure model assessment, is the case where the values of S^* and R are known from a direct numerical simulation or physical experiment. The fixed-point equations for the state variables yield the corresponding values of $\tilde{P}/\varepsilon$, $\tilde{P}_\theta/\varepsilon_\theta$, G_{13}/ε and G/ε. This result is dependent on the pressure–strain rate and pressure–scrambling models, but independent of the particular form of the modelled ε and ε_θ evolution equations. However, the equilibrium fixed-point analysis yields results that are identical to the long-time solution of a system of evolution equations for the Reynolds stresses and heat fluxes that include the k, k_θ, ε and ε_θ evolution equations. While both the k and k_θ equations are exact (for these homogeneous flows), their corresponding dissipation rate equations are modelled. The consistency of the ε equation has long been established for such homogeneous flows, whereas the ε_θ equation is not as well established. If needed, the

current analysis can then be used to better formulate improvements to this equation based on its performance in such homogeneous flows.

5.3. *Buoyant plane strain flow*

In this example, the deformation is aligned along the (x_1, x_3)-axes with $W = 0(\mathscr{R}^2 = 0)$, $S_{11} = -S$ and $S_{33} = S$, and the applied temperature gradient vector is once again aligned with the gravitational vector. It should be pointed out that the same results would have been obtained if the signs of S_{11} and S_{33} were interchanged. The reason is that changing the sign does not affect the total strain deformation of the fluid element. Therefore, the present analysis will only examine the case given by $S_{11} = -S$ and $S_{33} = S$. With this mean velocity and thermal field, $\zeta_1 = 0$ as can be seen from (18); then $L_2^* = 0$ and L_1^* is reduced to

$$L_1^* = -a_6 L_1 = a_6 \left(\frac{G}{\varepsilon}\right) S^*. \tag{45}$$

Equation (27) can then be simplified to

$$\left[1 - \frac{4a_3^2}{3} g^2 S^{*2}\right] \left(\frac{\tilde{P}}{\varepsilon}\right) = 2gS^* \left[2a_1 S^* + a_6 \left(\frac{G}{\varepsilon}\right) \left(1 - \frac{2a_3}{3} g S^*\right)\right]. \tag{46}$$

The corresponding equation for (G/ε) can be obtained from (31) or (28) and is given by

$$\left[\frac{1}{a_\theta} + RS^* \left(C_S - \tfrac{1}{3} a_6 C_b g Ri S^*\right)\right] \left(\frac{G}{\varepsilon}\right) = -Ri \frac{C_b}{3} R \left[2 + a_3 g \left(\frac{\tilde{P}}{\varepsilon}\right)\right] S^{*2} + 2RC_{\bar{g}} \bar{g}_3^2 + \tfrac{1}{2} RC_b Ri \left(\frac{\tilde{P}}{\varepsilon}\right) S^*, \tag{47}$$

where a_θ is again given by (34). With $\tilde{P}/\varepsilon$ and G/ε determined from the solution of (46) and (47), the ratio $\tilde{P}_\theta/\varepsilon_\theta$ can be deduced from (33). Note that once again Ri is defined by (37); however, the mean velocity gradient used in the definition is now derived from the mean strain field.

In order to validate (46) and (47) and their respective solutions, the same pressure–strain rate and pressure–scrambling models used previously to validate the buoyant shear case are used here. Since, at equilibrium, the state variables are independent of the initial conditions, the same set of numerical values used to initialize the buoyant shear calculations are used in the plane strain case. The SSG/AD modelled equations (1), (10), (13), (14), (35) and (36) are once again solved for different values of Ri in the range 0 to 25. The long-time solution of these equations then yields equilibrium values for S^* and R that are used to determine the equilibrium values for $\tilde{P}/\varepsilon$, G/ε and $\tilde{P}_\theta/\varepsilon_\theta$ from (46), (47) and (33), respectively. These equilibrium results are compared in figures 3(a) to 3(c) with the corresponding values obtained from the long-time numerical solutions of SSG/AD in the range $0 \leqslant Ri \leqslant 25$. The plots show that the equilibrium state variables, $\tilde{P}/\varepsilon$, G/ε and $\tilde{P}_\theta/\varepsilon_\theta$, asymptote to constant values for large Ri. The asymptote is reached at around $Ri = 10$ for $\tilde{P}/\varepsilon$ and $\tilde{P}_\theta/\varepsilon_\theta$, but approximately at $Ri = 20$ for G/ε. As in the buoyant shear flow case, both the long-time numerical solution and the equilibrium fixed-point analysis yield identical results. It should be noted that the non-isothermal plane strain case corresponds to the point $Ri = 0$. Since this limit is achieved by letting density become constant ($\beta = 0$) while maintaining Θ_3 finite, (47) yields the trivial solution $G/\varepsilon = 0$, and $\tilde{P}_\theta/\varepsilon_\theta$ depends on $\tilde{P}/\varepsilon$ and R alone. The resulting relation is given by (33) with $(G/\varepsilon) = 0$.

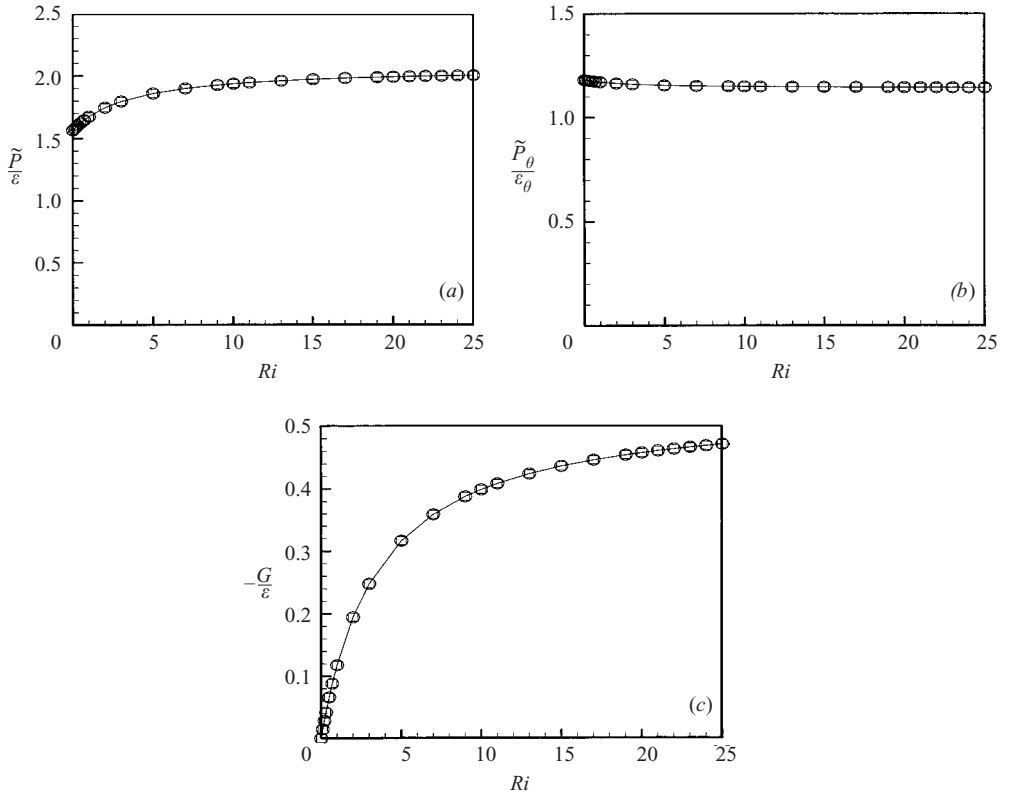

FIGURE 3. Equilibrium-state variation of (*a*) $\tilde{P}/\varepsilon$, (*b*) $\tilde{P}_\theta/\varepsilon_\theta$ and (*c*) $-(G/\varepsilon)$ with Ri for buoyant strain flows: —□—, SSG/AD model solution; —○—, analytical solution.

5.4. *Buoyant uniform flow*

The case of a mean uniform flow is of dynamical interest in the study of buoyant homogeneous turbulence. Two buoyant situations arise: the stable and the unstable case. Only the stably stratified case is considered here since the unstable case will most likely not lead to equilibrium turbulence. In a stably stratified uniform flow, three different forces are competing for influence. They are the inertia, viscous and buoyant forces (Komori *et al.* 1983; Metais & Herring 1989; Lienhard & Van Atta 1990; van Haren, Staquet & Cambon 1994). The interplay between the inertia and buoyant forces would give rise to an exchange of energy between k and k_θ. As a result, counter-gradient fluxes would develop to keep the energy budget in balance (Lienhard & Van Atta 1990; van Haren *et al.* 1994). In turn, this would lead to oscillations in the evolution of the Reynolds normal stress aligned with the gravity vector, the temperature variance, and the turbulent vertical heat flux (Stillinger *et al.* 1983; van Haren *et al.* 1994). Therefore, stable stratification inhibits mixing and leads to the development of counter-gradient fluxes and the onset of internal gravity waves. In view of this, equilibrium turbulence characterized by the fixed points $\dot{b}_{ij} = 0$ and $\dot{\zeta}_i = 0$ would most likely not exist for this flow. In order to further confirm the absence of such fixed points, the SSG/AD modelled evolution equations (1), (10), (13), (14), (35) and (36) are solved numerically with $\boldsymbol{S} = \boldsymbol{W} = 0$ to calculate the stably stratified case treated by van Haren *et al.* (1994). They considered two different cases of stable stratification, characterized by $N = \pi/3$ and π. The initial conditions specified

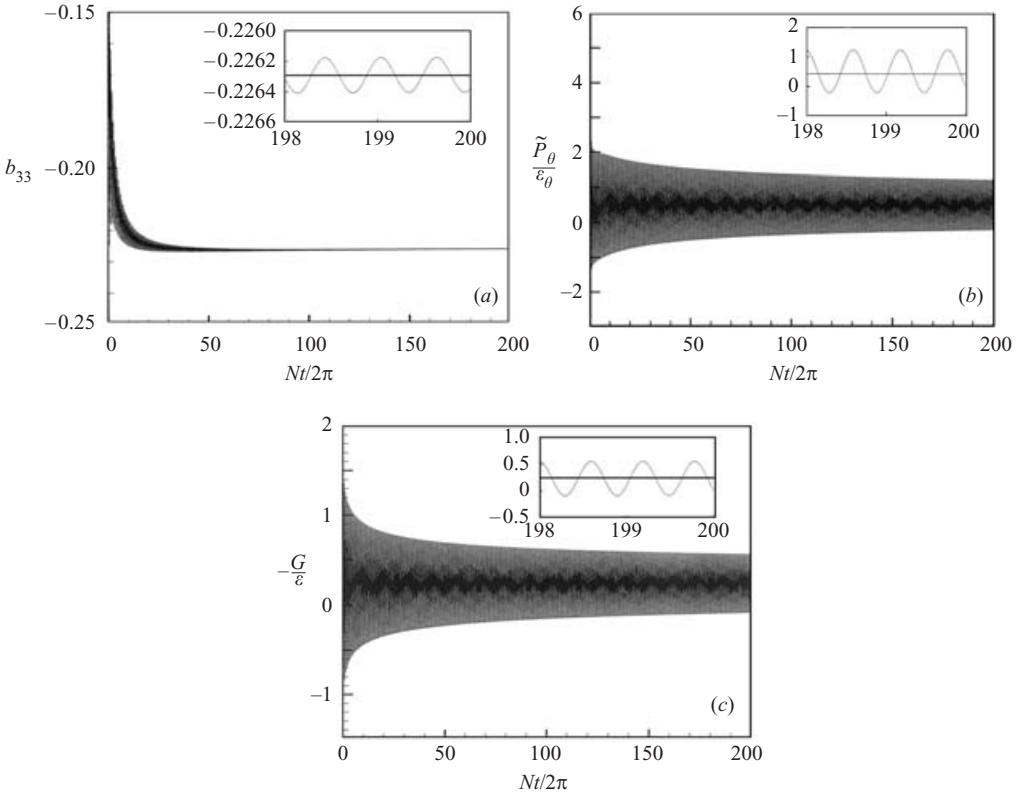

FIGURE 4. Variation of (*a*) b_{33}, (*b*) $\tilde{P}_\theta/\varepsilon_\theta$ and (*c*) $-(G/\varepsilon)$ with $Nt/2\pi$ for stably stratified uniform flows.

in van Haren *et al.* (1994) are used here and the calculations have been carried out to a non-dimensional time of $Nt/2\pi = 200$, far longer than that given by van Haren *et al.* (1994). For details concerning the calculations, see e.g. So *et al.* (1999). Sample plots of b_{33}, $\tilde{P}_\theta/\varepsilon_\theta$ and $-(G/\varepsilon)$ versus $Nt/2\pi$ are given in figures 4(*a*)–4(*c*) respectively. They clearly show that b_{33}, $\tilde{P}_\theta/\varepsilon_\theta$ and $-(G/\varepsilon)$ are still oscillating for large time (see the inset in each figure showing the variation of the parameter with a blown-up time coordinate). It is clear that b_{33}, $(\tilde{P}_\theta/\varepsilon_\theta)$ and $-(G/\varepsilon)$ oscillate with fairly constant amplitude. The observed trend is that the oscillations will persist for an even longer time, thus suggesting that equilibrium turbulence characterized by the fixed points $\dot{b}_{ij} = 0$ and $\dot{\zeta}_i = 0$ does not exist for such stably stratified uniform flow. This behaviour is true irrespective of whether the time coordinate is normalized by $2\pi/N$ or by k_o/ε_o.

5.5. *Invariant plane mapping of buoyant homogeneous turbulence*

It is of interest to quantify the effect of buoyancy on the turbulent velocity field. One of the best means of doing this is to examine the invariant map of the Reynolds stress anisotropies $2II_b = -\{\boldsymbol{b}^2\}$ and $3III_b = \{\boldsymbol{b}^3\}$ (Lumley 1978). Figure 5 shows the behaviour of these invariants for the cases of buoyant shear flow, buoyant plane strain flow and buoyant uniform flow obtained from the numerical solution of (1), (10), (13), (14), (35) and (36) for the respective cases. Calculations were carried out for $N = \pi/3$–50π for the uniform flow case, $Ri = 0$–~ 2 for the pure shear flow case

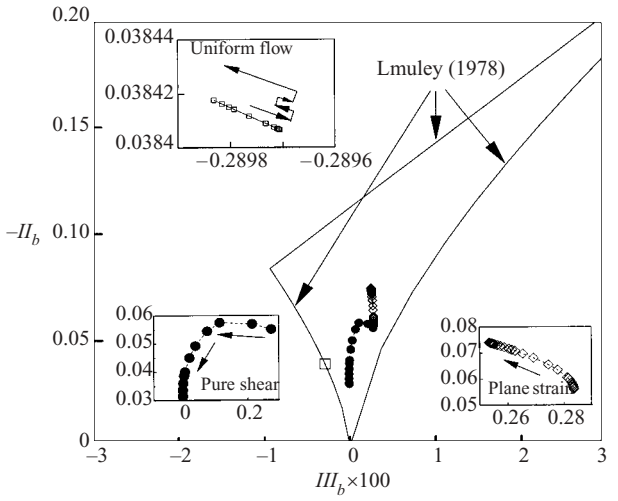

FIGURE 5. Invariant map $(III_b, -II_b)$ of equilibrium values for buoyant homogeneous turbulence as a function of Ri and N. For the pure shear case, $0 \leqslant Ri < 2$; for the plane strain case, $0 \leqslant Ri \leqslant 25$; while for the uniform flow case, $\pi/3 \leqslant N \leqslant 50\pi$.

and $Ri = 0$–25 for the plane strain case. Insets within the figure show the details of the variations for the three cases and the arrows indicate the directional behaviour as Ri or N increases. The effect of increasing Ri is clearly seen for the buoyant shear flow case. As Ri increases, the turbulent anisotropy decreases and there is a trend toward the isotropic limit (origin) of the invariant map. For this case, as Ri increases, the buoyant time scale becomes much shorter than the shearing time scale and a rapid-distortion limit is approached. Therefore, the rapid distortion in this case implies that the effects of buoyancy dominate the dynamics.

In contrast, the case of plane strain shows much less effect on the turbulence with increasing Ri even though the mean temperature gradient is once again aligned along the direction of the gravitational vector and a direction of straining motion as well. This shows that the effect of a pure straining motion in the mean velocity field inhibits the return-to-isotropy effects on the turbulent velocity field with increasing buoyancy. Even at $Ri = 25$, the buoyant plane strain value remains well within the realizable limits of the invariant map.

In the absence of any mean velocity gradients, a fixed-point equilibrium state does not exist and the turbulent velocity and thermal fields in the stable stratification case are characterized by oscillatory behaviour. Since there is only one Reynolds stress anisotropy component b_{33} directly affected by the buoyancy, the remaining kinetic energy is equally redistributed between the two remaining normal stress components and their anisotropies $b_{11} = b_{22}$ $(= -b_{33}/2)$. As figure 4(a) shows, $b_{33} < 0$, and this means that the turbulence anisotropies lie along the axisymmetric contraction boundary of the invariant map shown in figure 5. After a long time, oscillations still persist in all the state variables although the stress anisotropy oscillations are significantly less in amplitude than the corresponding $\tilde{P}_\theta/\varepsilon_\theta$ and $-(G/\varepsilon)$ levels. At this point, even with the (weak) oscillations, the turbulent velocity field dynamics is fixed along the invariant map boundary but with no identifiable trend toward either the two-component or isotropic limits.

6. Comparison with DNS data

Having examined the behaviour of buoyant turbulence for the $\varphi = 0$ case at the fixed points $\dot{b}_{ij} = \dot{\zeta}_i = 0$, the next step is to attempt to verify the calculations by comparing them with DNS and/or experimental data. Among the pure shear, plane strain and the uniform flow cases investigated, it was found that equilibrium as defined by the fixed points $\dot{b}_{ij} = \dot{\zeta}_i = 0$ does not exist for the case of a uniform flow with stable stratification. The reason is that b_{ij} as well as $\tilde{P}_\theta/\varepsilon_\theta$ and $-(G/\varepsilon)$ still oscillates with time even for $t = 400\pi/N$. Thus, equilibrium state variables for stably stratified flow cannot be determined. Since the present work is not about modelling, the evolution of b_{ij} and ζ_i is not calculated and not available for comparison with DNS and/or experimental data (Itsweire *et al.* 1986; Gerz *et al.* 1989; van Haren *et al.* 1994). A study on the modelling prediction of equilibrium states of buoyant shear and uniform flow has been carried out in Zhao *et al.* (2001). The effects of pressure–strain models, anisotropic dissipation rate modells and ε_θ equation modelling were studied in detail. Therefore, this aspect of predicting equilibrium states will not be repeated here. For plane strain flow, to the best of the authors' knowledge, DNS and/or experimental data on the equilibrium state do not appear to be available. Consequently, comparison of the present calculations is carried out with shear flow data only.

Recently, direct numerical simulations were carried out on homogeneous buoyant turbulent flow to investigate the evolution of turbulence in a uniformly sheared and in a non-vertical-shear medium (Jacobitz *et al.* 1997; Jacobitz & Sarkar 1998; Shih *et al.* 2000). Among the three studies, Jacobitz *et al.* (1997) and Jacobitz & Sarkar (1998) reported on the turbulence field, on the growth rate of k, and on the behaviour of the flux Richardson number Ri_f, which is defined as the ratio of the buoyant production to the shear production of k. On the other hand, the work of Shih *et al.* (2000) is an attempt to verify the findings of Jacobitz *et al.* (1997) that the stationary Richardson number depends on both the Reynolds number and the dimensionless shear number. Since the work of Jacobitz & Sarkar (1998) covered non-vertical as well as vertical shear, their DNS data are selected for comparison with the present calculation. Two cases are selected and these are given by $\varphi = 0$ and $\pi/2$. In these two cases, the mean flow is still two-dimensional and the present calculations can be straightforwardly performed without having to reformulate the equations for three-dimensional flows.

Since the equations for $\tilde{P}/\varepsilon$, $-(G/\varepsilon)$ and G_{13}/ε for the $\varphi = 0$ case have already been given, i.e. (38)–(40), only equations for the $\varphi = \pi/2$ case need be derived again. These equations can be deduced from (27)–(31) by noting that $\varphi = \pi/2$ in (25*a*). For this case $G_{13} = 0$, and therefore only equations for $\tilde{P}/\varepsilon$ and $-(G/\varepsilon)$ are required; $\tilde{P}_\theta/\varepsilon_\theta$, is still given by (33). Omitting the details, the resulting equations and Ri are given by

$$Ri \equiv -\beta\, g_3 \left(\frac{\partial \Theta}{\partial x_3}\right)\left(\frac{\partial U_1}{\partial x_2}\right)^{-2} = \frac{\bar{g}\,\Theta_3}{S^{*2}}, \tag{48}$$

$$L_1^* = L_2^* = 0, \tag{49}$$

$$L_3^* = \{\boldsymbol{L}^*\boldsymbol{S}^{*2}\} = a_6\left(\frac{G}{\varepsilon}\right)\{\boldsymbol{F}\boldsymbol{S}^{*2}\} = \tfrac{2}{3}a_6\Pi_S^*\left(\frac{G}{\varepsilon}\right), \tag{50}$$

$$\left[1 + g^2 S^{*2}\left(a_2^2 - \tfrac{1}{3}a_3^2\right)\right]\left(\frac{\tilde{P}}{\varepsilon}\right) - \tfrac{2}{3}a_3 a_6 g^2 S^{*2}\left(\frac{G}{\varepsilon}\right) = g a_1 S^{*2}, \tag{51}$$

	Equilibrium values of b_{ij} for $\varphi = 0$ case	$Ri = 0$		$Ri = 0.1$		$Ri = 0.2$	
		Present calculation	DNS data	Present calculation	DNS data	Present calculation	DNS data
(*a*)	b_{11}	0.19406	0.21986	0.22232	0.25926	0.23776	0.31322
	b_{22}	−0.05245	−0.05674	−0.03876	−0.07407	−0.02097	−0.08333
	b_{33}	−0.14161	−0.16312	−0.18355	−0.18519	−0.21680	−0.22989
	b_{13}	−0.15794	−0.160	−0.11616		−0.06330	−0.032
(*b*)	b_{11}	0.19406	0.21986	0.23347	0.31602	0.25880	0.34591
	b_{22}	−0.14161	−0.16312	−0.13871	−0.19048	−0.13683	−0.22013
	b_{33}	−0.05245	−0.05674	−0.09476	−0.12554	−0.12197	−0.12579
	b_{13}	−0.15794	−0.160	−0.16157		−0.16338	−0.115

TABLE 1. Comparison of the calculated b_{ij} with the DNS data of Jacobitz & Sarkar (1998) for (*a*) the $\varphi = 0$ case and (*b*) the $\varphi = \pi/2$ case for different Ri.

	Ri_f	
Ri	Present calculation	DNS data
0.	0.	0.
0.05	0.077	0.06
0.10	0.16	0.11
0.15	0.25	0.16
0.20	0.33	0.225

TABLE 2. Comparison of the flux Richardson number Ri_f with the DNS data of Jacobitz & Sarkar (1998) for different Ri.

$$R\left(\frac{\tilde{P}}{\varepsilon} - 1 + \frac{G}{\varepsilon} + C_{1\theta}\right)\left(\frac{G}{\varepsilon}\right) = -\left(1 - a_3 g\frac{\tilde{P}}{\varepsilon} - 2a_6 g\frac{G}{\varepsilon}\right)\left(\tfrac{2}{3}RC_b Ri\, S^{*2}\right) + 2RC_{\bar{g}}\bar{\mathrm{g}}^2. \tag{52}$$

This set of equations and (38)–(40) together with (33) are used to solve the two cases of $\varphi = 0$ and $\pi/2$ reported in Jacobitz & Sarkar (1998). The initial conditions specified in Jacobitz & Sarkar (1998) were used to start the numerical calculation of the SSG/AD modelled equations once Ri is specified so that S^*, Θ_3 and R could be determined. The equilibrium values of S^*, Θ_3 and R thus obtained are then substituted into (33), (38)–(40) and (33), (51)–(52), respectively, for the $\varphi = 0$ and $\pi/2$ cases in order to solve for the equilibrium values of $\tilde{P}/\varepsilon$, $-(G/\varepsilon)$ and $\tilde{P}_\theta/\varepsilon_\theta$. According to Jacobitz & Sarkar (1998), the growth rate of k for the $\varphi = 0$ and $\pi/2$ case can be expressed as

$$\gamma = \frac{1}{Sk}\frac{\mathrm{d}k}{\mathrm{d}t} = \left(\frac{\tilde{P}}{Sk} + \frac{G}{Sk} - \frac{\varepsilon}{Sk}\right). \tag{53}$$

Therefore, once $\tilde{P}/\varepsilon$ and $-(G/\varepsilon)$ are known, γ can also be calculated and compared with DNS data. Furthermore, the equilibrium values of b_{ij} can be calculated from (20) once L_i^* are known from (24*a–c*), and $Ri_f = G/\tilde{P}$ can be determined also.

The results of these calculations are tabulated in tables 1 and 2 for comparison with the DNS data. In addition, plots of γ versus Ri for the $\varphi = 0$ and $\pi/2$ case

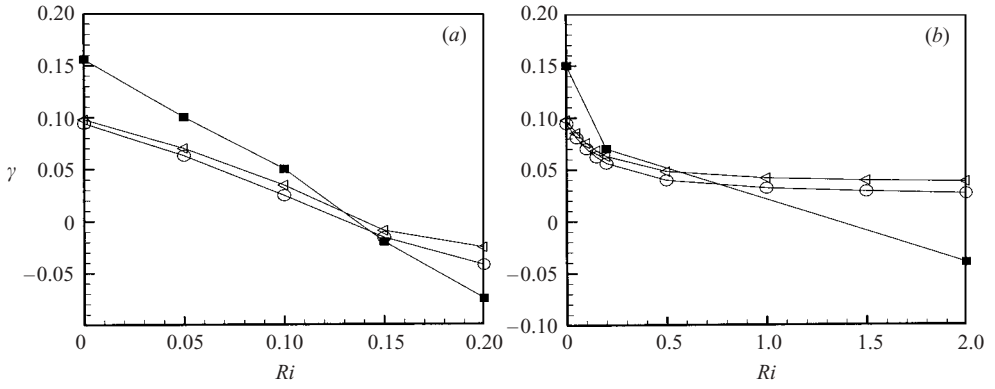

FIGURE 6. Comparison of the calculated γ with the DNS data of Jacobitz & Sarkar (1998) for different Ri: (*a*) $\varphi = 0$, (*b*) $\varphi = \pi/2$; —○—, present prediction evaluated at $St = 20$; —◁—, present prediction evaluated at $St = 200$; —■—, DNS data.

are shown in figures 6(*a*) and 6(*b*), respectively. In figure 6(*a*), the range of Ri is from 0 to 0.2, while it is from 0 to 2 in figure 6(*b*). The corresponding DNS data are also shown for comparison in figure 6. Note that there are only three points from the DNS data for the $\varphi = \pi/2$ case, so the interpolation between points should be interpreted with caution (figure 6*b*). Two curves for the calculated γ are plotted: one where the values of S^*, Θ_3 and R are determined at $St = 20$ and the other for corresponding values of S^*, Θ_3 and R evaluated at $St = 200$. A linear behaviour for γ within the range of Ri examined is reproduced for the $\varphi = 0$ case. If the critical Richardson number Ri_{cr} is defined by setting $\gamma = 0$ as suggested in Jacobitz *et al.* (1997), then the DNS data give $Ri_{cr} = 0.138$, while the analysis yields $Ri_{cr} = 0.130$ and 0.142 for $St = 20$ and 200, respectively (figure 6*a*). On the other hand, there is no Ri_{cr} predicted for the $\varphi = \pi/2$ case, whereas DNS data give a value of $Ri_{cr} = 1.36$ based on interpolation (figure 6*b*). The discrepancy could be due to the fact that the model constants used in SSG/AD were not calibrated against buoyant flow data. Therefore, the present methodology provides model developers with a more rational way to calibrate buoyant flow models. Overall, the predicted b_{ij} is in fair agreement with DNS data, so are the calculated Ri_f and γ. The discrepancy in b_{22} noted for the $\varphi = 0$ case and in b_{33} for the $\varphi = \pi/2$ case is because they are deduced from the calculated components of b_{ij} which has a zero trace.

These results showed that buoyancy effects on b_{ij} have been accounted for fairly well through $\boldsymbol{L}^*$ and the determination of the invariants $\{\boldsymbol{bS}^*\}$, $\{\boldsymbol{bW}^*\boldsymbol{S}^*\}$ and $\{\boldsymbol{bS}^{*2}\}$. All these are accomplished through a three-term representation for $\mathbf{b}$ as given in (20) and without solving any modelled ε and ε_θ evolution equations. The only models invoked are those for the pressure–strain tensor and the pressure–scrambling vector. If a representation for $\boldsymbol{b}$ is assumed that includes explicit terms for the buoyant flux, as suggested in So *et al.* (2002), an improved agreement with DNS data could be expected. It appears that equilibrium states have been reached asymptotically as early as $St = 20$ because the difference between the two different plots of the calculated γ is very small (figure 6). Based on these comparisons, for $Ri \leqslant 0.2$ it can be said that the present analytical prediction of the equilibrium states is in fair agreement with DNS data for the homogeneous buoyant shear flow where the mean shear gradient does not necessarily lie on the same plane as the mean temperature gradient.

7. Conclusions

A procedure developed previously for analysing the equilibrium state behaviour for non-buoyant turbulent homogeneous flows has been extended to the turbulent buoyant flow case. State variables have been extracted for the first time from algebraic relationships of scalar invariants formed from the Reynolds stress anisotropy tensor, the kinematic strain rate and rotation rate tensors, and a buoyant flux tensor. For the general case of two-dimensional homogeneous buoyant turbulent flow, five equivalent scalar equations were deduced from the Reynolds stress anisotropy equation and the scaled heat flux equation. A sixth equation to close the set was derived from the evolution equations for the turbulent kinetic energy and the temperature variance. These equations can be reduced to a set of four for the cases of non-isothermal homogeneous shear flow and buoyant shear flow, and a set of three equations for the case of buoyant plane strain flow. The limiting cases of pure shear and pure strain in the absence of buoyancy were also recovered correctly.

One immediate result of the derived algebraic equations is that R does not appear in any of these equations except that for $(\tilde{P}_\theta/\varepsilon_\theta)$, which is consistent with the general linearity principle of Pope (1983) for scalar flux modelling.

For the case of non-isothermal homogeneous shear flows, the velocity field is decoupled from the thermal field, but not the other way around. Therefore, an examination of the limiting behaviour given by Θ_3 going to zero leads to the conclusion that in the modelling of the pressure–scrambling vector, the coefficient $C_{3\theta}$ should be zero. This result has been obtained previously by Wikstrom *et al.* (2000) who carried out an elaborate model evaluation to show that $C_{3\theta}$ should be zero, whereas the analysis used here extracted this result from an analysis of the equations for state variables valid at equilibrium. This highlights the value of the current methodology since it can aid in the development of the proper closure models without recourse to extensive numerical validation tests.

In this non-isothermal homogeneous shear flow case, seven equilibrium state parameters can be identified and they are $\tilde{P}/\varepsilon$, $\tilde{P}_\theta/\varepsilon_\theta$, S^*, ζ_1, ζ_3, Θ_3, and R. There are four independent algebraic equations and they can be solved for $\tilde{P}/\varepsilon$, $\tilde{P}_\theta/\varepsilon_\theta$, ζ_1, and ζ_3, once S^*, Θ_3, and R are specified from the numerical modelling solution. An analysis of these equations also leads to the conclusion that the closure coefficient $C_{3\theta}$ that appeared in the modelled pressure–scrambling term must be zero.

For a buoyant turbulent shear flow, seven equilibrium state variables can be identified. The Richardson number Ri appears as a dimensionless parameter in the scalar equations; however, with known values of the imposed mean velocity and temperature gradients it is a given parameter defining the problem and not an equilibrium parameter. Thus, the independent set of state variables can be identified as $\tilde{P}/\varepsilon$, $\tilde{P}_\theta/\varepsilon_\theta$, k/ε, G/ε, G_{13}/ε, k/k_θ, and R (with knowledge of R and k/k_θ, the ratio $\varepsilon/\varepsilon_\theta$ is also known.). The four algebraic equations, (33), (38), (39) and (40), can be solved to give the variation of the equilibrium values for $\tilde{P}/\varepsilon$, $\tilde{P}_\theta/\varepsilon_\theta$, G/ε, and G_{13}/ε, with Ri, provided values of S^*, $\bar{g}_3$ (i.e. k/k_θ or $\varepsilon/\varepsilon_\theta$), and R are specified. These specified values can be obtained from the long-time numerical solution of the modelled evolution equations (1), (10), (13), (14), (35) and (36). Since the algebraic equations and modelled evolution equations were closed using the same pressure–strain and pressure–scrambling models both sets of equations give identical results. It is worth noting that while a self-consistent set of equations and methodologies has been established for the equilibrium case, it is not possible at this time to verify the accuracy of these values. Only with experimental and/or numerical simulation (DNS

or LES) results at equilibrium can one assess whether the equilibrium values for state variables are correct. Once such physical and/or numerical results are obtained, the validity of the proposed models, particularly the model closure coefficients, can be assessed. This would be particularly true of the modelled ε_θ equation since it has not been studied as thoroughly as the other modelled equations. As was discussed extensively by Zhao *et al.* (2001), numerous models for this equation have been proposed over the years.

For the case of buoyant flow with pure strain, $G_{13}/\varepsilon = 0$ so there are now six independent equilibrium state variables: $\tilde{P}/\varepsilon$, $\tilde{P}_\theta/\varepsilon_\theta$, k/ε, G/ε, k/k_θ, and R. Three algebraic equilibrium equations are available for the solution of the three variables $\tilde{P}/\varepsilon$, $\tilde{P}_\theta/\varepsilon_\theta$ and G/ε provided values of S^*, $\bar{g}_3$ (i.e. k/k_θ or $\varepsilon/\varepsilon_\theta$), and R are specified. Once again, these specified values could be obtained from the long-time numerical solution of the SSG/AD model. The values of $\tilde{P}/\varepsilon$, $\tilde{P}_\theta/\varepsilon_\theta$, and G/ε thus determined are again found to be identical to those obtained from the numerical modelling solution. In the case of stably stratified buoyant flow, no equilibrium state characterized by the fixed points $\dot{b}_{ij} = 0$ and $\dot{\zeta}_i = 0$ exists; however, at long time the flow field variables, $\tilde{P}_\theta/\varepsilon_\theta$, G/ε, and b_{33}, display a near constant oscillatory behaviour.

These results, from the pure shear, plane strain and uniform flow cases, provide a unique mapping of the turbulence dynamics for buoyant flows. In each of the three cases, the effect of increasing Ri or N is different. For the pure shear case the trend is toward isotropy. The turbulent Reynolds stress invariants are much less affected in the plane strain case. The model predictions in this case remain realizable over the entire Ri range examined, but the trend is away from isotropy. As for the uniform flow case, stably stratified turbulence was found to yield anisotropy invariants that lie along the axisymmetric contraction boundary for all levels of stratification.

Finally, a comparison has been made with DNS data of buoyant turbulence with nonvertical shear. Specifically, two cases are considered, one with $\varphi = 0$ and another with $\varphi = \pi/2$. The calculated b_{ij}, Ri_f and γ are in fair agreement with available DNS data. Furthermore, the predicted Ri_{cr} is in good agreement with DNS data for the $\varphi = 0$ case.

R.M.C.S. and T.B.G. acknowledge support (Grants PolyU5154/99E and PolyU5169/01E) given to them by the Research Grants Council, The Government of the HKSAR. L.H.J. acknowledges support given to her while on leave from Tsinghua University by HK PolyU.

Appendix

With the quadratic term in (21)–(23) omitted ($a_4 = 0$), these equations can be rewritten in the form (cf. Jongen & Gatski 1998)

$$\left[\frac{1}{g^2} + 4\Pi_S^* \left(\tfrac{1}{3}a_3^2 - a_2^2\mathscr{R}^2\right)\right] \{\boldsymbol{bS}^*\} = \frac{1}{g}\left[2a_1\Pi_S^* - L_1^* - 2a_2 g L_2^* + 2a_3 g L_3^*\right], \quad \text{(A 1)}$$

$$\{\boldsymbol{bW}^*\boldsymbol{S}^*\} = 2a_2 g \Pi_S^* \mathscr{R}^2 \{\boldsymbol{bS}^*\} - g L_2^*, \quad \text{(A 2)}$$

$$\left\{\boldsymbol{bS}^{*2}\right\} = \tfrac{2}{3}a_3 g \Pi_S^* \{\boldsymbol{bS}^*\} - g L_3^*, \quad \text{(A 3)}$$

where L_1^*, L_2^*, and L_3^* are given by (24). From (24) it can be seen that the additional unknowns $[\bar{g}_i \zeta_j S_{ji}^*]$ and $[\bar{g}_i \zeta_j W_{jk}^* S_{ki}^*]$ now appear, and the equations governing these scalar invariants need to be constructed from the scaled heat flux vector equation (18).

These scalar invariant equations are then given by

$$-\frac{1}{a_\theta}\left[\bar{g}_i\zeta_k S^*_{ki}\right] + RC_S\Pi^*_S\left[\bar{g}_i\zeta_k\delta^{(2d)}_{ki}\right] + RC_\Omega\left[\bar{g}_i\zeta_k W^*_{kl}S^*_{li}\right]$$
$$= RC_b\left(\frac{2}{3} - \frac{\{\boldsymbol{bS}^{*2}\}}{\Pi^*_S}\right)\left[\bar{g}_i\Theta_k S^*_{ki}\right] + 2RC_{\bar{g}}\left[\bar{g}_i\bar{g}_k S^*_{ki}\right]$$
$$+RC_b\{\boldsymbol{bS}^*\}\left[\bar{g}_i\Theta_k\delta^{(2d)}_{ki}\right] - RC_b\frac{\{\boldsymbol{bW}^*\boldsymbol{S}^*\}}{\Pi^*_S\mathscr{R}^2}\left[\bar{g}_i\Theta_k W^*_{ki}\right], \quad (A\,4)$$

$$-\frac{1}{a_\theta}\left[\bar{g}_i\zeta_k W^*_{kl}S^*_{li}\right] - RC_S\left[\bar{g}_i\zeta_k W^*_{ki}\right]\Pi^*_S + RC_\Omega\left[\bar{g}_i\zeta_k S^*_{ki}\right]\Pi^*_S\mathscr{R}^2$$
$$= RC_b\left(\frac{2}{3} - \frac{\{\boldsymbol{bS}^{*2}\}}{\Pi^*_S}\right)\left[\bar{g}_i\Theta_k W^*_{kl}S^*_{li}\right] + 2RC_{\bar{g}}\left[\bar{g}_i\bar{g}_k W^*_{kl}S^*_{li}\right]$$
$$-RC_b\{\boldsymbol{bS}^*\}\left[\bar{g}_i\Theta_k W^*_{ki}\right] + RC_b\{\boldsymbol{bW}^*\boldsymbol{S}^*\}\left[\bar{g}_i\Theta_k\delta^{(2d)}_{ki}\right], \quad (A\,5)$$

$$-\frac{1}{a_\theta}\left[\bar{g}_i\zeta_k W^*_{ki}\right] + RC_S\left[\bar{g}_i\zeta_k W^*_{kl}S^*_{li}\right] + RC_\Omega\Pi^*_S\mathscr{R}^2\left[\bar{g}_i\zeta_k\delta^{(2d)}_{ki}\right]$$
$$= RC_b\left(\frac{2}{3} - \frac{\{\boldsymbol{bS}^{*2}\}}{\Pi^*_S}\right)\left[\bar{g}_i\Theta_k W^*_{ki}\right] + 2RC_{\bar{g}}\left[\bar{g}_i\bar{g}_k W^*_{ki}\right]$$
$$-RC_b\frac{\{\boldsymbol{bS}^*\}}{\Pi^*_S}\left[\bar{g}_i\Theta_k S^*_{kl}W^*_{li}\right] - RC_b\frac{\{\boldsymbol{bW}^*\boldsymbol{S}^*\}}{\Pi^*_S}\left[\bar{g}_i\Theta_k S^*_{ki}\right], \quad (A\,6)$$

where the equation for the invariant $[\bar{g}_i\zeta_j W^*_{ji}]$ is also required for closure. Equations (A 4)–(A 6) are not independent equations and can be related to one another through factors involving the components of the strain rate and rotation rate tensors. The exact relationship is dependent on the particular flow under investigation and for this reason the equations are left in the form given. In the buoyant case, with the explicit coupling of the equations shown in (A 1)–(A 6) and the implicit coupling through the modelling variable $g = g(\tilde{P}/\varepsilon, G/\varepsilon)$, it is necessary to not only account for the dependence on $\tilde{P}/\varepsilon$ but also to account for the dependence on G/ε $(= -\bar{g}_3\zeta_3)$. The ratio G/ε is determined directly from (18) and is

$$\frac{1}{a_\theta}\left(\frac{G}{\varepsilon}\right) - RC_S\left[\bar{g}_i\zeta_k S^*_{ki}\right] + RC_\Omega\left[\bar{g}_i\zeta_k W^*_{ki}\right] = RC_b\left(\frac{2}{3} + \frac{2\{\boldsymbol{bS}^{*2}\}}{\Pi^*_S}\right)[\bar{g}_i\Theta_i]$$
$$+2RC_{\bar{g}}[\bar{g}_i\bar{g}_i] - RC_b\frac{\{\boldsymbol{bS}^*\}}{\Pi^*_S}\left[\bar{g}_i\Theta_k S^*_{ki}\right] + RC_b\frac{\{\boldsymbol{bW}^*\boldsymbol{S}^*\}}{\Pi^{*2}_S\mathscr{R}^2}\left[\bar{g}_i\Theta_k W^*_{kl}S^*_{li}\right]$$
$$-3RC_b\frac{\{\boldsymbol{bS}^{*2}\}}{\Pi^*_S}\left[\bar{g}_i\Theta_k\delta^{(2d)}_{ki}\right]. \quad (A\,7)$$

It should be pointed out that equations (A 1)–(A 7) are only valid for two-dimensional flows where the mean velocity gradient makes an angle $\varphi = 0$ or $\pi/2$ with the (x_1, x_3)-plane. Furthermore, (A 1)–(A 7) provide a set of seven equations for the seven unknowns $\{\boldsymbol{bS}^*\}$, $\{\boldsymbol{bW}^*\boldsymbol{S}^*\}$, $\{\boldsymbol{bS}^{*2}\}$, $[\bar{g}_i\zeta_k S^*_{ki}]$, $[\bar{g}_j\zeta_k W^*_{kl}S^*_{lj}]$, $[\bar{g}_i\zeta_k W^*_{ki}]$ and (G/ε),

respectively. From the relations for the velocity and temperature gradients introduced in (25) and (26), further reductions of these rather general forms are discussed starting with (27).

REFERENCES

Abid, R. & Speziale, C. G. 1993 Predicting equilibrium states with Reynolds stress closures in channel flow and homogeneous shear flow. *Phys. Fluids* A **5**, 1776–1782.

Craft, T. J. & Launder, B. E. 1989 A new model for the pressure/scalar-gradient correlation and its application to homogeneous and inhomogeneous free shear flows. *7th Symp. on Turbulent Shear Flows, Stanford, CA*, Paper 12–4.

Gerz, T. & Schumann, U. 1991 Direct simulation of homogeneous turbulence and gravity waves in sheared and unsheared stratified flows. In *Turbulence Shear Flows* (ed. F. Durst *et al.*), pp. 27–46. Springer.

Gerz, T., Schumann, U. & Elghobashi, S. E. 1989 Direct numerical simulation of stratified homogeneous turbulent shear flow. *J. Fluid Mech.* **200**, 563–594.

van Haren, L., Staquet, C. & Cambon, C. 1994 A study of decaying stratified turbulence by a two-point closure EDQNM model and by direct numerical simulations. *Proc. 14th Intl Symp. on Stratified Flows, Grenoble, France, June 26–July 2.*

Itsweire, E. C., Helland, K. N. & Van Atta, C. W. 1986 The evolution of grid-generated turbulence in a stably stratified fluid. *J. Fluid Mech.* **162**, 299–338.

Ivey, G. N. & Imberger, J. 1991 On the nature of turbulence in a stratified fluid, part I: the energetics of mixing. *J. Phys. Oceanogr.* **21**, 650–658.

Jacobitz, F. G. & Sarkar, S. 1998 The effect of nonvertical shear on turbulence in a stably stratified medium. *Phys. Fluids* **10**, 1158–1168.

Jacobitz, F. G., Sarkar, S. & Van Atta, C. W. 1997 Direct numerical simulations of the turbulence evolution in a uniform sheared and stably stratified flow. *J. Fluid Mech.* **342**, 231–261.

Jones, W. P. & Musonge, P. 1988 Closure of the Reynolds-stress and scalar flux equations. *Phys. Fluids* **31**, 3589–3604.

Jongen, T. & Gatski, T. B. 1998 A new approach to characterizing the equilibrium states of the Reynolds stress anisotropy in homogeneous turbulence. *Theor. Comput. Fluid Dyn.* **11**, 31–47, and erratum **12**, 71–72.

Kaltenbach, H. J., Gerz, T. & Schumann, U. 1994 Large-eddy simulation of homogeneous turbulence and diffusion in stably stratified shear flow. *J. Fluid Mech.* **280**, 1–40.

Kolmogorov, A. N. 1941 The local structure of turbulence in an incompressible viscous fluid for very large Reynolds numbers. *C. R. Acad. Sci. USSR* **30**, 301; English transl.: *Turbulence, Classic Papers on Statistical Theory* 1961 (ed. S. K. Friedlander & L. Topper). Interscience.

Komori, S., Ueda, H., Ogino, F. & Mizushina, T. 1983 Turbulence structure in stably stratified open-channel flow. *J. Fluid Mech.* **130**, 13–26.

Launder, B. E. 1973 Scalar property transport by turbulence. *Rep.* HTS/73/26. Mechanical Engineering, Imperial College, London.

Launder, B. E. 1978 Heat and mass transport. In *Topics in Applied Physics* (ed. P. Bradshaw), pp. 231–287. Springer.

Launder, B. E. 1988 On the computation of convective heat transfer in complex turbulent flows. *J. Heat Transfer* **110**, 1112–1128.

Launder, B. E. 1989 The prediction of forced-field effects on turbulent shear flow via second-moment closure. In *Advances in Turbulence 2* (ed. H. H. Fernholz & H. E. Fiedler), pp. 338–358. Springer.

Leuchter, O. & Benoit, J. P. 1991 Study of coupled effects of plane strain and rotation on homogeneous turbulence. In *Eighth Symp. On Turbulent Shear Flows, Technical University of Munich.*

Lienhard, J. H. & Van Atta, C. W. 1990 The decay of turbulence in thermally stratified flow. *J. Fluid Mech.* **210**, 57–112.

Lumley, J. L. 1978 Computational modeling of turbulent flows. *Adv. Appl. Mech.* **18**, 123–176.

Metais, O. & Herring, J. R. 1989 Numerical simulation of freely evolving turbulence in stably stratified fluids. *J. Fluid Mech.* **202**, 117–148.

Monin, A. S. 1965 On the symmetry of turbulence in the surface shear layer of air. *Atmos. Ocean. Phys.* **1**, 45–54.

Nagano, Y. & Shimada, M. 1996 Development of a two-equation heat transfer model based on direct simulations of turbulent flows with different Prandtl numbers. *Phys. Fluids* **8**, 3379–3402.

Piccirillo, P. & Van Atta, C. W. 1997 The evolution of a uniformly sheared thermally stratified turbulent flow. *J. Fluid Mech.* **334**, 61–86.

Pope, S. B. 1983 Consistent modeling of scalars in turbulent flows. *Phys. Fluids* **26**, 404–408.

Reynolds, W. C. 1990 The potential and limitations of direct and large-eddy simulations. In *Whither Turbulence? Turbulence at the Crossroads* (ed. J. L. Lumley). Lecture Notes in Physics, vol. 357, pp. 313–343. Springer.

Rivlin, R. S. & Ericksen, J. L. 1955 Stress-deformation relations for isotropic materials. *Arch. Rat. Mech. Anal.* **4**, 323–425.

Rogallo, R. S. & Moin, P. 1984 Numerical simulation of turbulent flows. *Annu. Rev. Fluid Mech.* **16**, 99–137.

Rohr, J. J., Itsweire, E. C., Helland, K. N. & Van Atta, C. W. 1988 Growth and decay of turbulence in a stably stratified shear flow. *J. Fluid Mech.* **195**, 77–111.

Shabany, Y. & Durbin, P. A. 1997 Explicit algebraic scalar flux approximation. *AIAA J.* **35**, 985–989.

Shih, L. H., Koseff, J. R., Ferziger, J. H. & Rehmann, C. R. 2000 Scaling and parameterization of stratified homogeneous turbulent shear flow. *J. Fluid Mech.* **412**, 1–20.

Sirivat, A. & Warhaft, Z. 1983 The effect of a passive cross-stream temperature gradient on the evolution of temperature variance and heat flux in grid turbulence. *J. Fluid Mech.* **128**, 323–346.

So, R. M. C. & Speziale, C. G. 1999 A review of turbulent heat transfer modeling. In *Annual Review of Heat Transfer, X* (ed. C. L. Tien), pp. 177–219. Begell House.

So, R. M. C., Vimala, P., Gatski, T. B. & Zhao, C. Y. 2002 Accounting for buoyancy effects in explicit algebraic stress models: homogeneous turbulent shear flows. *Theor. Comput. Fluid Dyn.* **16**, 1–20.

So, R. M. C., Zhao, C. Y. & Gatski, T. B. 1999 Predicting buoyant shear flows using anisotropic dissipation rate model. *J. Flow, Turbulence Combust.* **63**, 193–221.

Sommer, T. P. & So, R. M. C. 1995 On the modeling of homogeneous turbulence in a stably stratified flow. *Phys. Fluids* **7**, 2766–2777.

Sommer, T. P., So, R. M. C. & Zhang, J. 1997 Modeling nonequilibrium and history effects of homogeneous turbulence in a stably stratified medium. *Intl J. Heat Fluid Flow* **18**, 29–37.

Speziale, C. G. 1991 Analytical methods for the development of Reynolds stress closures in turbulence. *Annu. Rev. Fluid Mech.* **23**, 107–157.

Speziale, C. G. & Mac Giolla Mhuiris, N. 1989 On the prediction of equilibrium states in homogeneous turbulence. *J. Fluid Mech.* **209**, 591–615.

Speziale, C. G., Sarkar, S. & Gatski, T. B. 1991 Modelling the pressure–strain correlation of turbulence: an invariant dynamical systems approach. *J. Fluid Mech.* **227**, 245–272.

Stillinger, D. C., Helland, K. N. & Van Atta, C. W. 1983 Experiments on the transition of homogeneous turbulence to internal waves in a stratified fluid. *J. Fluid Mech.* **131**, 91–122.

Tavoularis, S. & Corrsin, S. 1981 Experiments in nearly homogeneous turbulent shear flows with a uniform mean temperature gradient. Part 1. *J. Fluid Mech.* **104**, 311–347.

Wikstrom, P. M., Wallin, S. & Johansson, A. V. 2000 Derivation and investigation of a new explicit algebraic model for the passive scalar flux. *Phys. Fluids* **12**, 688–702.

Youssef, M. S., Nagano, Y. & Tagawa, M. 1992 A two-equation heat transfer model for predicting turbulent thermal fields under arbitrary wall thermal conditions. *Intl J. Heat Mass Transfer* **35**, 3095–3104.

Zhao, C. Y., So, R. M. C. & Gatski, T. B. 2001 Turbulence modeling effects on the prediction of the equilibrium states of buoyant shear flows. *Theor. Comput. Fluid Dyn.* **14**, 399–422.